Marine and Petroleum Geology 134 (2021) 105342

Contents lists available at ScienceDirect

Marine and Petroleum Geology

journal homepage: www.elsevier.com/locate/marpetgeo

Upper Jurassic to Lower Cretaceous source rocks in the Norwegian Barents Sea, part I: Organic geochemical, petrographic, and paleogeographic investigations

Andrés Cedeño [a,*], Sverre Ohm [a], Alejandro Escalona [a], Dora Marín [a], Snorre Olaussen [b], Thomas Demchuk [c]

[a] University of Stavanger, Norway
[b] The University Centre in Svalbard, Norway
[c] Louisiana State University, USA

ARTICLE INFO

Keywords:
Source rock
Organofacies variations
Barents Sea
Macerals
Carbon isotopes
Generation potential

ABSTRACT

This study provides a subregional to regional characterization of organofacies changes within the two members of the Upper Jurassic to Lower Cretaceous Hekkingen Formation (i.e. Alge and Krill) by integrating geochemical and petrographic analysis with paleogeographic models.

The gross kerogen composition of the Hekkingen Formation is dominated by terrestrial macerals. This preponderance of land-derived particles is more pronounced in the Krill Member than in the underlying Alge Member. There is a greater proportion of marine macerals within distal areas of the Hammerfest Basin and well 7218/1-S in the southern Bjørnøyrenna Fault Complex. This shift in the relative proportion of marine and terrestrial macerals is ascribed to changes in the location of the depositional sites with respect to the sources of the terrestrial materials.

The Alge Member features the highest levels of total organic carbon (TOC $\geq$7 wt %), but the more discrete and organically poorer beds of the Krill Member still remain sufficiently rich to be considered petroleum source rocks (TOC $\geq$2 wt %). Hydrogen indices (HI) between 50 and 400 mg HC/g TOC recorded throughout the entire formation indicate that the kerogen within both members has similar oil and gas generation capabilities. These low to moderate HI values are indicative of immature Type III to II-III kerogens and are generally consistent with the high proportions of terrestrial macerals. Prior to thermal maturation, marine type II kerogens (i.e. $\leq$ 400 mgHC/gTOC) probably existed in the marine liptinite-rich rocks in the distal Hammerfest Basin and Bjørnøyrenna Fault Complex. At least three factors controlled the detected variability in geochemical parameters: dilution rates of organic matter, varying inputs of terrestrial versus marine organic matter, and the degree of preservation. The documented variability in organic-rich facies assists in reducing source rock risk in the study area, but also helps explorationists understand source rock distribution across other shelfal areas.

1. Introduction

During the Late Jurassic, high rates of organic carbon burial and petroleum source rock formation were globally widespread (Leith et al., 1993; Klemme, 1994; Weissert and Mohr, 1996; Berner and Kothavala, 2001). Upper Jurassic deposits of the Hanifa-Arab Formation in the Arabian-Iranian Basin, the Bazhenov Formation in West Siberia, the Smackover and Taman formations in the Gulf of Mexico, and the Kimmeridgian Shale in the Northwestern European Shelf are prime archives of increased accumulation of organic carbon leading to prolific source rocks (Klemme, 1994). Most of these shale and carbonate units are characterized by the occurrence of type II organic matter (Klemme, 1994) resulting from a significant rise in global eustatic sea level and widespread establishment of epicontinental seas in coexistence with the advent of skeletonized planktonic organisms (Klemme, 1994).

The Hekkingen Formation, stratigraphically equivalent to the Kimmeridgian Shale, records intensified carbon productivity and sedimentation within a Late Jurassic epeiric sea in the Norwegian Barents Sea

* Corresponding author.
E-mail address: andres.f.cedenomotta@uis.com (A. Cedeño).

https://doi.org/10.1016/j.marpetgeo.2021.105342
Received 9 April 2021; Received in revised form 31 August 2021; Accepted 22 September 2021
Available online 29 September 2021

(Worsley, 2008; Henriksen et al., 2011a; Marin et al., 2020) (Fig. 1A). As a unit, it extends from the Tromsø Basin northwards into the Bjarmeland Platform (Fig. 1B) and the Svalbard Archipelago, where it is named the Agardhfjellet Formation. The Hekkingen Formation consists of a lower succession (i.e. Alge Member) of black shales featuring the highest total organic carbon (TOC) values, and an upper succession (i.e. Krill Member) of siltstones featuring lower TOC values (Dalland et al., 1988; Mørk et al., 1999; Henriksen et al., 2011a; Georgiev et al., 2017). Rock-Eval hydrogen indices (HI) in both members are seen to be highly variable at the same maturity level (i.e. same Tmax in Fig. 2). The documented variability in organic matter quantity and quality suggests that the Hekkingen Formation is not a homogenous entity and contains varying proportions of marine and terrestrial kerogens. This condition implies paleogeographic and palaeoceanographic controls on deposition of the sedimentary organic matter. As with this study, previous geochemical work, using analogous analytical data has also documented source rock variability within this formation (Bjorøy et al., 1983; Smelror et al., 2001; Ohm et al., 2008; Henriksen et al., 2011a; Abay et al., 2017; Helleren et al., 2020).

Rock-Eval and TOC analysis constitute the conventional approach to assessing the total generative potential of petroleum source rocks and predicting the nature of their kerogen. Importantly, this chemical approach lacks the qualitative information of the organic precursors (i.e. macerals or organic matter type) provided by maceral microscopic analysis and disregards the inorganic aspects of the sediment matrix. The purpose of this paper is to characterize subregional to regional organofacies variations within the Hekkingen Formation in relationship to paleoenvironmental and paleogeographic conditions by integrating geochemical and petrographic analyses with paleogeographic models. Through implementing this integrated approach, this study augments the earlier geochemical work that recognized variations in organofacies within the Hekkingen Formation and provides the basis for assessing changes in the petroleum generative potential (see Cedeño et al., 2021). The latter has direct implications for prospectivity studies of the southwestern Barents Sea.

2. Structural and stratigraphic framework

Multiple studies have recognized the Middle Jurassic to Early Cretaceous as a period of renewed tectonic activity in the southwestern Barents Sea characterized by extensional and strike slip faulting, halokinesis, and uplift of local highs (Sund et al., 1986; Berglund et al., 1986; Faleide et al., 1993; Gernigon et al., 2014; Serck et al., 2017; Rojo et al., 2019; Kairanov et al., 2021). Tectonic activity concentrated mostly along local to semi-regional fault complexes such as Troms-Finnmark, Ringvassøy-Loppa, Bjørnøyrenna, Nysleppen, and Hoop (Fig. 1B). These diachronous fault systems controlled subsidence of the basins (i.e. Hammerfest, Tromsø, Bjørnøya, Nordkapp, and Fingerdjupet) and uplift of the structural highs (Clark et al., 2014; Blaich et al., 2017; Indrevær et al., 2017; Mulrooney et al., 2017; Serck et al., 2017; Kairanov et al., 2019; Faleide et al., 2019; Tsikalas et al., 2021). From the Cretaceous to the Holocene, the greater Barents Sea region underwent different magnitudes of uplift and erosion (Riis, 1996; Doré et al., 2000; Cavanagh et al., 2006; Henriksen et al., 2011b). The combined effects of the opening of the Atlantic and Artic oceans and the Pliocene-Pleistocene glacial-interglacial cycles have resulted in net

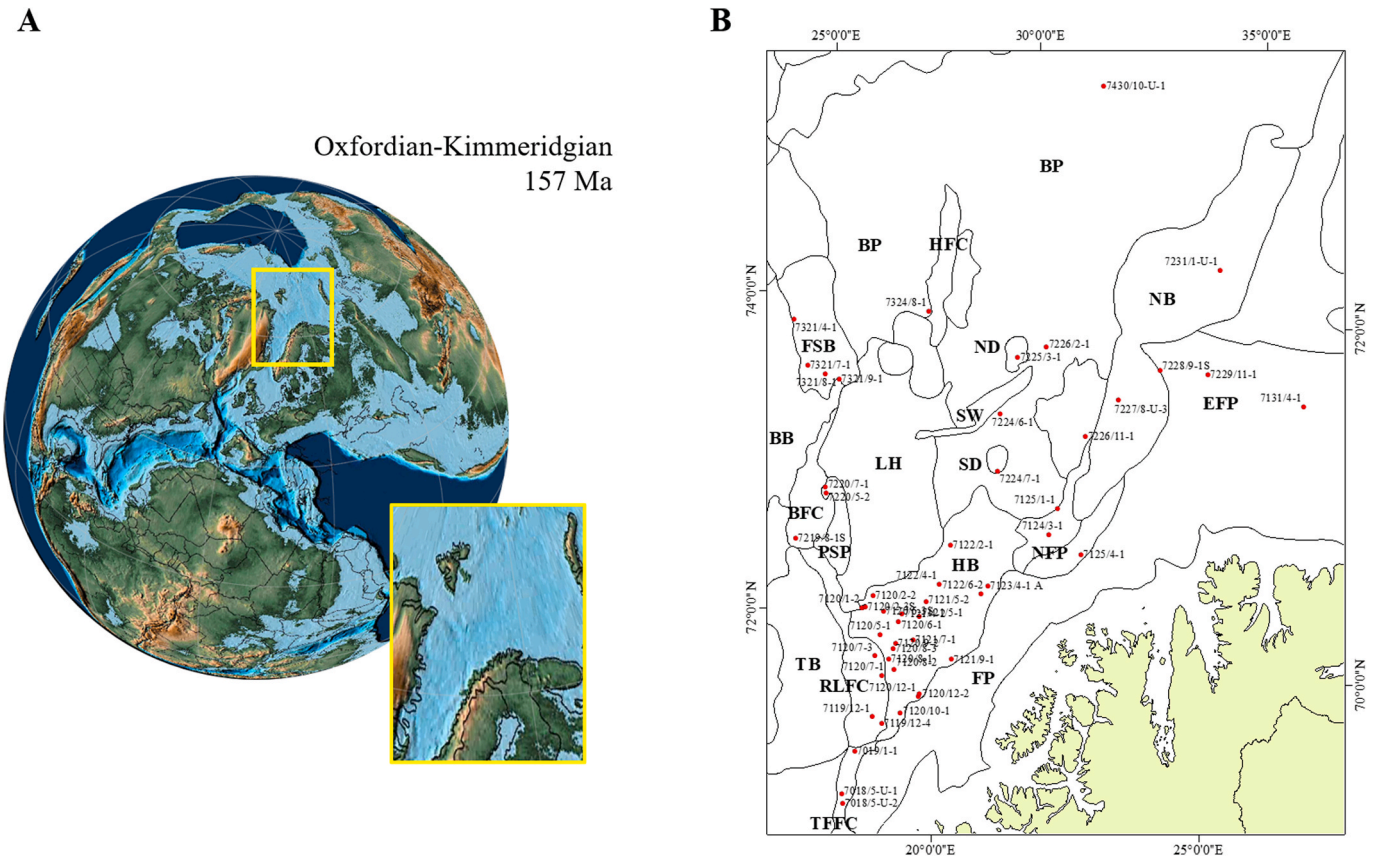

Fig. 1. A. Paleogeographic location of the Barents Sea within the northwestern European Shelf at the Oxfordian-Kimmeridgian boundary (Paleomap Project; Scotese, 2016). **B.** Map of the southwestern Barents Sea displaying the main structural elements and wells used in this study. BP= Bjarmeland Platform, HFC= Hoop Fault Complex. MB = Maud Basin, MH = Mercurius High, NB= Nordkapp Basin, EFP = eastern Finnmark Platform, ND= Norvarg Dome, SG= Swaen Graben, SD= Samson Dome, FSB= Fingerdjupet Sub-basin, BB= Bjørnøya Basin, BFC= Bjørnøya Fault Complex, PSP= Polhem Sub-platform, LH = Loppa High, NFC= Nysleppen Fault Complex, HB= Hammerfest Basin, CH= Central High, RLFC = Ringvassøy-Loppa Fault Complex, TB = Tromsø Basin, FP= Finnmark Platform, TFFC = Troms--Finnmark Fault Complex.

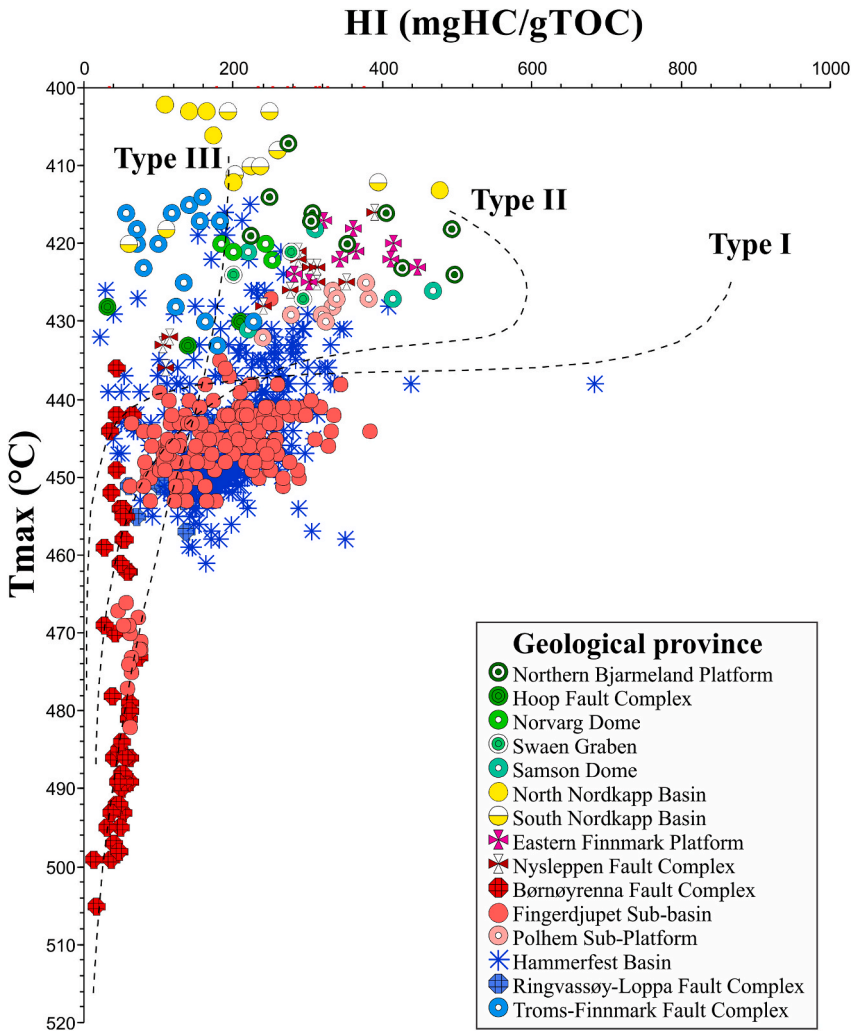

Fig. 2. Hydrogen index (HI) versus Tmax Rock-Eval (Tmax) plot of samples from the Hekkingen Formation. Samples from this study and from the IGI (Integrated Geochemical Interpretations) database are plotted. Maturation pathways for the three main kerogen types are shown after Cornford (1988). Samples are color-coded based on geological provinces. (For interpretation of the references to color in this figure legend, the reader is referred to the Web version of this article.)

erosion values varying from 0 to more than 3000 m (Faleide et al., 1984; Riss and Fjeldskaar, 1992; Johansen et al., 1992; Knies et al., 2009; Henriksen et al., 2011b).

During the Late Jurassic, most of the Barents Sea shelf was flooded, and deposition was controlled by regional transgression and gradual landwards migration of the shorelines (Henriksen et al., 2011a; Marin et al., 2020). The Late Jurassic is known to be a period of global eustatic sea level rise and high burial rates of organic carbon in the oceans (Schlanger and Jenkyns, 1976; Weissert et al., 1979; Leith et al., 1993; Klemme, 1994; Weissert and Mohr, 1996; Georgiev et al., 2017).

Several aspects of Late Jurassic geological and oceanographic conditions are manifest in the sedimentary record of the Barents Sea. The Oxfordian marks a clear lithological shift from the silty-mudstones and marls of the Fuglen Formation to the organic-rich shales of the Hekkingen Formation (Dalland et al., 1988; Mørk et al., 1999; Smelror et al., 2001; Henriksen et al., 2011a). A widespread middle Oxfordian hiatus is known to record this mineralogical shift (Bugge et al., 2002; Smelror et al., 2001; Wierzbowski and Smelror, 2020). Contiguous units on the Russian shelf include the Bazhenov Formation in the South Barents Sea, Timan Pechora, and West Siberian basins (Grace and Hart, 1986; Gavshin and Zakharov, 1996; Henriksen et al., 2011a).

The Hekkingen Formation consists of two members according to the TOC content and well log character: the Alge Member and the overlying Krill Member (Fig. 3). Biostratigraphically controlled age dates indicate a Late Oxfordian? To late Kimmeridgian age for the Alge Member and a Kimmeridgian to Ryazanian age for the Krill Member (Dalland et al., 1988; Georgiev et al., 2017; Mørk et al., 1999; Smelror et al., 2001). Costa and Davey (1992) and Smelror and Below (1993) argued that the Alge rocks in the Polhem Sub-platform are slightly older, spanning from Callovian to early Kimmeridgian. The boundary between these two units is interpreted as diachronous (Leith et al., 1993; Marín et al., 2020), i.e. its age and stratigraphic position may vary across the different structural provinces. The top of the Hekkingen Formation is informally known as the Base Cretaceous Unconformity, a hiatus ranging in age from Kimmeridgian to early Barremian (Århus, 1991; Bugge et al., 2002; Marín et al., 2018; Wierzbowski and Smelror, 2020).

The Alge Member is composed of black shale and typically displays high gamma ray (GR) values (Fig. 3). Geochemical and elemental analysis show that this member contains the highest levels of TOC (Ohm et al., 2008; Henriksen et al., 2011a; Abay et al., 2017). The Alge Member varies in thickness from 185 m (well 7129/8-1-s) in the Bjørnøyrenna Fault Complex to around 35 m in the Hammerfest Basin (Mørk et al., 1999; Marín et al., 2020). Localized sand injectites and thin turbiditic sandstone have been described along the boundary between the Hammerfest Basin and the Bjørnøyrenna Fault Complex and in the Bjørnøya Basin (Dalland et al., 1988; Mørk et al., 1999; Smelror et al., 2001; Bugge et al., 2002; Henriksen et al., 2011a; Helleren et al., 2020). Mørk et al., (1999) interpret the Alge Member to have been laid down

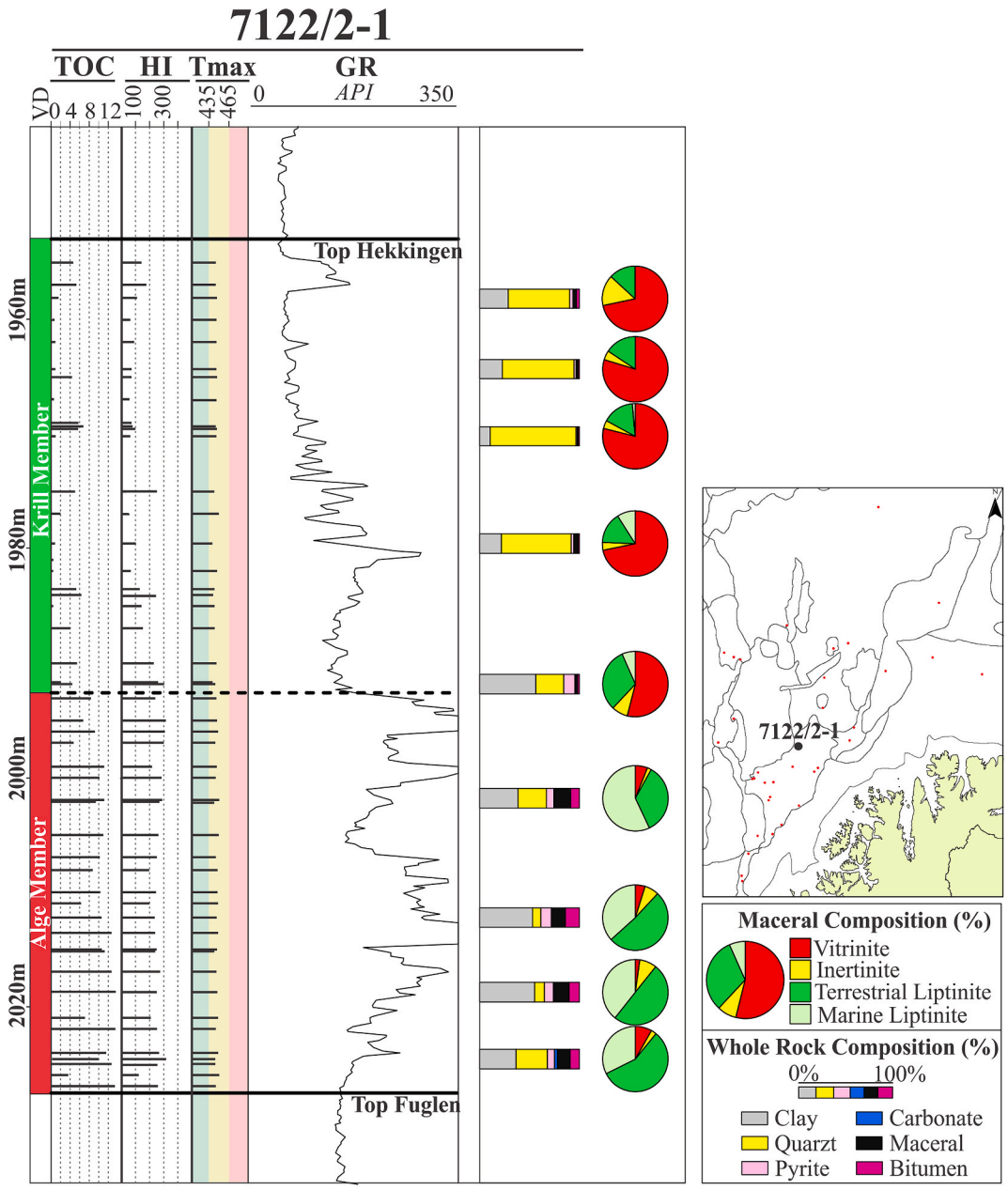

Fig. 3. Typical gamma ray (GR) log of the Hekkingen Formation at well 7122/2-1 displaying source rock analytical data (i.e. TOC, Tmax, HI). Mineral and maceral compositions of studied samples at different depths are also shown.

within a shelf environment with anoxic bottom water conditions. Helleren et al., (2020) recognize short phases of more oxygenated bottom water during deposition of this member.

The Krill Member consists of silt, silty shales, and very fine sand. Total organic carbon values within this member are diminished relative to the underlying Alge Member (Mørk et al., 1999; Ohm et al., 2008; Henriksen et al., 2011a; Abay et al., 2017). The thickness of the Krill Member varies considerably across the Barents Sea, from more than 600 m within the Bjørnøyrenna Fault Complex to virtually absent in some wells of the Hammerfest Basin (Marín et al., 2020). Deposition of this unit is interpreted to have occurred in a wide range of water depth conditions ranging from shallow shelf to possibly deep marine systems (Mørk et al., 1999; Marín et al., 2020). Variations in paleobathymetric conditions and thickness of the Krill Member were controlled by widespread tectonic activity (Marín et al., 2020). Around the buried Mjølnir crater, the Upper Volgian-Ryazanian Ragnarok Formation and the Sindre Bed consist of breccias, pebbles, sand, and mud ejected by the Mjørnir impact (Gudlaugsson, 1993; Tsikalas et al., 1999; Dypvik et al., 2004).

3. Materials and methods

3.1. Thickness maps

The thickness map for each of the members was built using publicly available well log data retrieved from the Diskos data base (NPD, 2021). To calculate sedimentary rates, a one-dimensional decompaction process was carried out using the Sclater-Christie equation $\phi(z) = \phi_0 e^{-CZ}$, where $\phi(z)$ is the porosity at any depth, ϕ_0 is the depositional porosity of a lithology, c is the porosity depth coefficient (km^{-1}), and z is depth (m). ϕ_0 values were adopted from the North Sea study by Sclater and Christie (1980). The shale-rich sediments of the Alge Member were assigned a $\phi_0 = 0.63$, whereas a lower value of 0.56 (an average between sand $\phi_0 = 0.49$ and shale $\phi_0 = 0.63$) was assigned to the siltier sediments of the

Krill Member. The compaction curves employed to back-calculate initial thicknesses are considered to be an exponential relationship as defined by Sclater and Christie (1980). All present-day depths were corrected to account for the Late Cretaceous-Holocene erosion using the regional map of net erosion by Henriksen et al. (2011b).

3.2. Sample material

The rock material used in this research includes a total of 320 conventional core and drilling cutting samples from 35 oil and stratigraphic (i.e. IKU Stratigraphic Drilling Projects) wells located across the southwestern Barents Sea (Fig. 1; Table 1). Sample material was collected from the Norwegian Petroleum Directorate (NPD) and the SINTEF well repositories in Stavanger and Trondheim, Norway, respectively. The sampled intervals were selected based on the stratigraphic boundaries of the Hekkingen Formation as defined by the NPD and preexisting geochemical studies from well completion reports. Sample selection was designed to ensure regular sampling intervals and prioritize core material over cuttings.

3.3. Chemical analyses

All samples described in section 3.2. were divided into subsets; one sample subset for organic geochemical studies (i.e. TOC, Rock-Eval, and isotope analysis) and the other sample subset for microscopy (i.e. organic and inorganic components). For geochemical analysis, all samples were mechanically ground to powder. A split of the powdered sample was treated with hydrochloric acid to remove carbonate minerals and combusted in a LECO SC-632 oven. The amount of carbon in the sample was measured as carbon dioxide by an IR-detector. A second split of the powdered sample was pyrolyzed using a Rock-Eval 6 instrument, allowing direct measurement of free hydrocarbons (S_1), remaining hydrocarbon generative potential (S_2), carbon dioxide (CO_2) content produced during thermal cracking (S_3), and temperature of S_2 maxima (T_{max}). The pyrolysis programme started at 300 °C (held for 3 min) and increased to 650 °C (held for 0 min) at 25 °C/min.

The remaining portion of selected powdered samples was used for measuring the carbon isotopic composition ($\delta^{13}C$) of the saturate, aromatic, and asphaltene (i.e. SARA) fractions. Isolation of the extractable organic matter (EOM) was performed using a Soxtec Tecator instrument. Thimbles were pre-extracted in dichloromethane with 7 % (vol/vol) methanol, 10 min boiling and 20 min rinsing. The sample was weighed accurately in the pre-extracted thimbles and boiled for 1 h and rinsed for 2 h in approximately 80 cc of dichloromethane with 7 % (vol/vol) methanol. Copper blades activated in concentrated hydrochloric acid were added to the extraction cups to cause free sulfur to react with the copper.

For deasphaltening, extracts were evaporated almost to dryness before a small amount of dichloromethane (3 times the amount of EOM) was added. Pentane was added in excess (40 times the volume of EOM and dichloromethane) and the solution was stored for at least 12 h in a dark place before the solution was filtered or centrifuged and the weight of the asphaltenes measured. The deasphaltened samples were then loaded into an automatic sampler and placed in a combustion reactor (Thermo Fisher Scientific Elemental Analyzer) held at 1020 °C. The produced water was trapped on Magnesium Perchlorate. CO_2 was separated by column and flashed into Delta V Plus Isotope Ratio Mass Spectrometer (IRMS, Thermo Fisher Scientific) via Conflo IV.

3.4. Petrographic analyses

The sample subset for microscopy was crushed and sieved through a 16-mesh sieve, and then embedded in thermoplastic epoxy in 2.54 cm molds. The pellets were ground and polished according to ASTM standards (ASTM, 2011). All samples were investigated under both white- and UV-light using a Zeiss Axio-Scope A1 at 500× (10× eyepiece, and 50× objective) in immersion oil. White- and UV-light was provided by an X-Cite 120 LED light source. Point-counts were conducted using a proprietary automated point-counter attached to the stage of the Zeiss Axio-Scope. As macerals and minerals were identified under the cross-hairs in the field of view, data were captured using proprietary software: once the petrographer made a count, the computer and motorized stage would then automatically move step-wise to a new, random field of view. Three-hundred counts of macerals and minerals were made for each sample. If there was insufficient organic matter after the 300 counts, counting was continued until 100 total counts of organic matter were collected. The resolution of the microscope is 1 μm (≥1 μm).

4. Results

4.1. Thickness map and whole rock constituents

4.1.1. The Alge member

The thickness map of the Alge Member shows that sediments accumulated preferentially within downthrown blocks of the Bjørnøyrenna Fault Complex (Fig. 4A). Decompaction estimations for the 185 m shale-rich succession in well 7219/8-1 S yield an initial thicknesses of roughly 430 m, which equates to sedimentation rates of approximately 86 m per million years (m/Ma). An average decompacted thicknesses of 55 m is estimated for most of the Hammerfest Basin, whereas a slightly higher average thickness of 60 m is calculated for the southern portion of the Bjarmeland Platform, the Nordkapp Basin, and the eastern Finnmark Platform. These figures imply sedimentary rates of roughly 11 and 12 m/Ma, respectively.

The average whole rock composition (i.e. per well) of the Alge Member consists of, in descending order, clay, sand, organic particles (i.e. macerals and solid bitumen), pyrite, and carbonate grains (Table 1). The clay content varies between 31 % and 64 % and the quartz content between 9 and 50 %. The relative abundance of sand increases in the eastern margin of the Hammerfest Basin, the Nysleppen Fault Complex, the eastern Finnmark Platform, and around the Norvarg Dome (Fig. 4A). The total content of macerals ranges between 6 and 18 %, while the content of solid bitumen ranges from 5 to 26 % (Table 1). The average pyrite content, in the form of framboids, typically accounts for less than 10 %, but occasionally reach up to 18 % in individual samples.

4.1.2. The Krill Member

The thickness map of the Krill Member (Fig. 4B) reveals that the fault-controlled depocenter in the southern end of the Bjørnøyrenna Fault Complex continued to be active during the sedimentation of the Krill Member. A present-day thickness of up to 680 m in well 7219/8-1 S translates into roughly 1300 m of decompacted sediments, indicating sedimentation rates of up to 130 m/My. Another major north-east-south-west oriented depocenter, presently containing up to 310 m of sediments, developed along the Troms-Finnmark Fault Complex and extended over the southern half of the Hammerfest Basin. Decompaction of this succession yields an initial thickness of 540 m, implying a sedimentary rate of 54 m/My. The remaining western and northern areas of the Hammerfest Basin show a present-day average thickness of 40 m, which equates to a decompacted thicknesses of nearly 70 m and to a sedimentary rate of 7 m/My. Across the southern Bjarmeland Platform, the Krill Member exhibits an average thickness of about 35 m. This suggests that initial accumulation of over 55 m of clastic detritus occurred at a rate of around 6 m/My.

Sedimentary rates presented in the ongoing study are only approximate partly because of poor age control and partly because some of the wells used in this study were drilled in or around structural highs, where sedimentary units are thinner or eroded, or both. The Krill Member, for example, is known to have been partly eroded, at least locally, by the regionally-extended Base Cretaceous Unconformity. Either scenario could be advocated to explain the absence of the Krill Member in the Nordkapp Basin and the adjacent eastern Finnmark Platform.

Table 1
Well identification, whole rock constituents, maceral composition, and bulk source rock geochemical data (i.e. total organic carbon = TOC; hydrogen index = HI; Tmax Rock Eval = Tmax) of the studied wells discriminated by member. Composition and source rock data represent average values calculated for each well. Maceral compositions are shown in normalised percentage. NP= Hekkingen member is not present. Refer to Fig. 1 for abbreviations of geological provinces.

Well name	Geo. province	Alge member										
		Whole rock constituents						Normalised maceral composition %				TOC/Rock-Eval
		% Clay	% Quartz	% Pyrite	% Carbonates	% Macerals	% Bitumen	Marine Lip	Terres Lip	Inertinite	Vitrinite	TOC (wt %)
7018/5-U-1	TFFC	60	9	12	1	8	9	11	11	11	68	7
7018/5-U-2	TFFC	51	10	3	3	7	26	11	32	23	35	12
7019/1-1	RLFC	43	29	10	0	13	5	45	13	16	26	9
7119/12-1	RLFC	46	25	12	1	9	8	30	18	19	33	9
7120/1-2	HB	41	20	12	0	16	10	25	60	4	7	9
7120/10-1	HB	60	14	8	2	8	7	5	23	14	58	9
7120/12-1	HB	35	26	10	4	11	14	19	45	6	30	10
7120/2-2	HB	54	18	8	0	7	14	42	21	17	20	11
7120/2-3 S	HB	37	16	17	1	18	11	41	43	7	9	11
7120/6-3 S	HB	NP	NP	NP	NP	NP	NP	NP	NP	NP	NP	NP
7120/8-3	HB	54	11	11	0	10	14	35	15	19	31	12
7120/9-2	HB	31	30	11	0	13	14	62	9	9	20	10
7121/4-2	HB	35	14	16	3	13	20	69	7	7	16	10
7121/9-1	HB	40	32	9	1	12	7	25	34	10	32	9
7122/2-1	HB	46	20	8	1	15	11	41	48	5	5	11
7122/4-1	HB	44	12	12	3	10	18	45	9	21	25	10
7122/6-2	HB	50	12	9	1	10	19	11	37	21	31	12
7123/4-1 A	HB	41	36	1	0	11	11	31	35	12	24	11
7124/3-1	NFC	22	48	8	0	8	14	36	24	8	31	7
7125/1-1	NFC	14	7	2	8	26	0	32	25	16	26	13
7131/4-1	RFC	28	50	6	0	7	10	4	44	26	26	9
7219/8-1 S	BFC	42	20	7	2	11	17	53	13	20	14	7
7220/5-2	PSP	44	41	5	0	5	4	25	34	10	30	4
7224/6-1	ND	64	15	6	0	6	10	6	33	17	44	11
7224/7-1	SM	NP	NP	NP	NP	NP	NP	NP	NP	NP	NP	NP
7225/3-1	ND	40	38	7	0	6	9	7	13	20	61	9
7226/2-1	SG	48	31	2	0	7	12	10	35	31	24	8
7227/8-U-3	NB	52	12	7	1	8	20	27	43	14	17	12
7229/11-1	EFP	48	23	7	1	7	15	6	42	16	35	11
7231/1-U-1	NB	48	22	4	1	7	18	14	47	20	19	11
7321/7-1	FSB	45	26	7	1	5	17	5	4	23	67	9
7321/8-1	FSB	NP	NP	NP	NP	NP	NP	NP	NP	NP	NP	NP
7321/9-1	FSB	NP	NP	NP	NP	NP	NP	NP	NP	NP	NP	NP
7324/8-1	MH	NP	NP	NP	NP	NP	NP	NP	NP	NP	NP	NP
7430/10-U-1	BP	47	18	4	1	14	16	21	42	12	24	13

Compositionally, clay is the dominant constituent of the Krill Member in most of the Hammerfest Basin and the Ringvassøy-Loppa and Troms-Finnmark fault complexes with volume percentages of around 40 % or higher (Table 1; Fig. 4B). This clay-dominated composition contrasts with the significantly higher quartz content in the depocenter west of the Central High that reaches up to 89 %. In the most northernly parts of the Hammerfest Basin, the Fingerdjupet Sub-basin, and the Bjarmeland Platform, quartz is the predominant constituent. Similar proportions of clay and quartz particles occur in the Bjørnøyrenna Fault Complex. Total maceral content varies between 2 and 10 % whereas solid bitumen typically shows lower values than in the Alge Member, varying between 1 and 10 % (Table 1). Pyrite rarely constitutes 10 % of the whole rock.

4.2. Visual kerogen analysis

Under incident light microscopy, most of the organic materials (i.e. macerals + solid bitumen) in the studied samples appear to be recognizable as particles larger than the resolution of the microscope, i.e. ≥ 1 μm. This is substantiated by a correlation of the volume percentage of organics to the weight percentage of total organic carbon (TOC) in Fig. 5. As expected in the absence of large amounts of submicroscopic organic matter, the computed regression line for the dataset yields a roughly 2:1 relationship of the volume percentage of organics to the weight percentage of TOC (Scheidt and Littke, 1989).

The maceral analysis from kerogen microscopy indicates that both members contain significant proportions of terrestrial macerals, i.e. vitrinite and terrestrial-derived liptinites (Figs. 6 and 7; Table 1). Particles of vitrodetrinite and primary vitrinite constitute the bulk of the vitrinite group (Fig. 6A and B), but the relative abundance of the former is commonly triple that of the later. The terrestrial liptinite sub-group comprises mainly particles of sporinite, occasional cutinite, and rarely occurring resinite (Fig. 6G and H). Colonial alginite, also included in the terrestrial liptinite sub-group, corresponds to debris of lacustrine or shallow marine colonial algae of which *Botryococcus* is the most representative (Fig. 6E). The marine liptinite sub-group consists mainly of alginite particles (i.e. lamalginite, tasmanites, dinoflagellates; Fig. 6F); locally, fluorescing amorphinite occurs as the dominant marine maceral. Importantly, the composition of the various kerogen groups in samples of the Alge Member are overall similar to those in the Krill Member samples. This implies that sedimentary organic matter in the two members derived essentially from the same kinds of organisms, and that no significant or permanent changes occurred in the biota sourcing the organic matter during Alge and Krill times. The difference in the relative

Alge member		Krill member												
TOC/Rock-Eval		Whole rock constituents						Normalised maceral composition %				TOC/Rock-Eval		
HI (mgHC/gTOC)	Tmax (°C)	% Clay	% Quartz	% Pyrite	% Carbonates	% Macerals	% Bitumen	Marine Lip	Terres Lip	Inertinite	Vitrinite	TOC (wt %)	HI (mgHC/gTOC)	Tmax (°C)
117	416	54	28	5	1	7	5	12	28	7	53	3	128	426
181	417	54	21	8	2	5	10	7	24	8	61	5	127	419
122	449	43	41	5	0	8	3	34	15	11	40	4	139	450
113	452	56	26	9	0	4	4	19	12	16	52	3	172	448
203	432	5	89	4	0	2	0	6	11	3	80	1	111	438
184	418	42	32	9	1	10	6	12	30	9	49	5	200	422
266	423	41	34	12	1	7	6	9	52	16	22	6	321	428
175	448	59	16	8	0	9	8	24	42	14	21	4	199	448
260	434	NP	NP	NP	NP	NP	NP	NP	NP	NP	NP	NP	NP	NP
NP	NP	13	71	6	1	7	2	41	9	6	44	2	257	389
183	434	63	17	8	0	7	4	7	42	8	43	4	183	439
407	434	9	72	10	0	6	4	4	32	11	54	6	287	432
188	445	64	14	7	2	9	4	15	33	5	48	3	184	445
280	432	41	40	6	1	9	3	26	36	3	35	4	301	433
265	440	28	64	4	0	2	2	4	20	5	71	2	133	440
203	452	62	17	9	0	7	5	26	35	12	27	4	226	441
272	434	63	17	6	0	8	5	5	37	18	40	5	287	435
261	434	11	81	1	1	5	1	4	30	24	43	2	190	436
295	422	14	70	4	0	10	1	9	62	1	19	4	191	430
315	423	NP	NP	NP	NP	NP	NP	NP	NP	NP	NP	NP	NP	NP
361	322	NP	NP	NP	NP	NP	NP	NP	NP	NP	NP	NP	NP	NP
12	514	38	33	6	2	15	6	70	3	7	20	3	71	387
328	428	NP	NP	NP	NP	NP	NP	NP	NP	NP	NP	NP	NP	NP
238	423	43	49	3	0	4	1	0	17	36	47	4	293	427
NP	NP	39	29	9	2	12	9	28	45	9	18	3	290	424
250	421	NP	NP	NP	NP	NP	NP	NP	NP	NP	NP	NP	NP	NP
191	421	23	72	1	0	4	1	1	10	26	62	3	254	426
238	408	NP	NP	NP	NP	NP	NP	NP	NP	NP	NP	NP	NP	NP
373	422	NP	NP	NP	NP	NP	NP	NP	NP	NP	NP	NP	NP	NP
162	407	NP	NP	NP	NP	NP	NP	NP	NP	NP	NP	NP	NP	NP
61	477	NP	NP	NP	NP	NP	NP	NP	NP	NP	NP	NP	NP	NP
NP	NP	30	53	7	0	4	6	4	12	15	69	3	174	448
NP	NP	29	52	8	1	6	4	26	25	11	38	3	224	444
NP	NP	13	76	4	0	3	3	19	22	0	26	2	298	286
366	417	NP	NP	NP	NP	NP	NP	NP	NP	NP	NP	NP	NP	NP

abundance of macerals groups is ascribed instead to changes in the location of the depositional sites with respect to the sources of the terrestrial materials.

4.2.1. Northern areas: Bjarmeland and eastern Finnmark platforms and Nordkapp Basin

Fig. 7 shows the general distribution of the maceral groups across the study area. High concentrations of vitrinitic and terrestrial liptinitic macerals are characteristic of the Alge Member samples in the southern Bjarmeland and eastern Finnmark platforms (Figs. 7A and 8D). Inertinite is the next most abundant maceral and marine liptinitic particles are only of subordinate abundance (i.e. $\leq$10 %; Table 1). The overlying Krill Member is virtually depleted of marine debris with only localized occurrences in the Samson Dome and the area between the Maud Basin and the Hoop Fault Complex (Figs. 7B and 8D). The Alge Member in the eastern Finnmark Platform is, compared with the southern Bjarmeland, richer in terrestrial liptinites. The maceral composition of the Alge samples within the Nordkapp Basin is slightly enriched in marine liptinites relative to the surrounding platforms (Fig. 7A).

4.2.2. Central-southern areas: Hammerfest Basin, Ringvassøy-Loppa and Troms-Finnmark fault complexes

The Alge Member along the south-west-north-east boundary of the Finnmark Platform exhibits varying maceral assemblages overall dominated by land-derived particles (Fig. 7A; Table 1). The organic fraction in the southern portion of this boundary, i.e. Troms-Finnmark Fault Complex and the southern end of the Hammerfest Basin, consists mostly of vitrinites and terrestrial liptinites (Fig. 9A). The content of inertinites rarely exceeds 15 % and only trace amounts of marine liptinites occur. Stratigraphically equivalent sediments in the eastern Hammerfest Basin (Fig. 9B) and northwards in the Nysleppen Fault Complex show a higher content of liptinitic material (Fig. 7A). Nevertheless, the Alge Member in the Nysleppen Fault Complex is richer in marine liptinites than it is in the eastern and northeastern Hammerfest Basin. The amount of marine macerals increases considerably in the central and western areas of the Hammerfest Basin and moderately in the Ringvassøy-Loppa Fault Complex (Figs. 7A and 9C-D; Table 1). The average content (i.e. per well) of marine liptinites commonly exceeds 30 % and reaches distinctively high values of up to 65 % in the central parts of the Hammerfest Basin. Vitrinitic material constitutes the main terrestrial input and only rarely exceeds 25 %. Grains of finely disseminated alginite dominate the marine organic fraction. Only in the wells

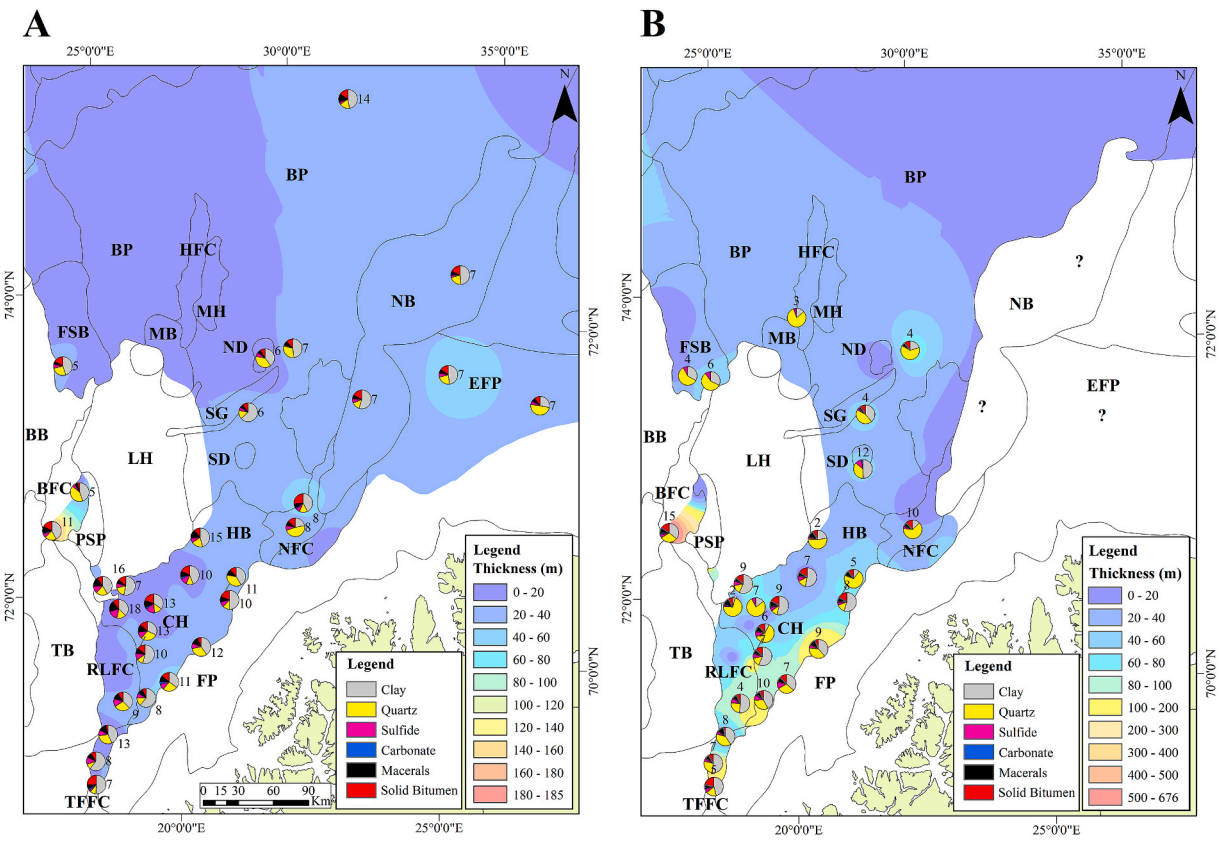

Fig. 4. Thickness maps of the Alge (**A**) and Krill (**B**) members. The pie diagrams represent the average (i.e. per well) whole rock compositions calculated from the microscopic analyses. Accompanying labels represent the average volume percentage of macerals in the whole rock. See Table 1 for the plotted values.

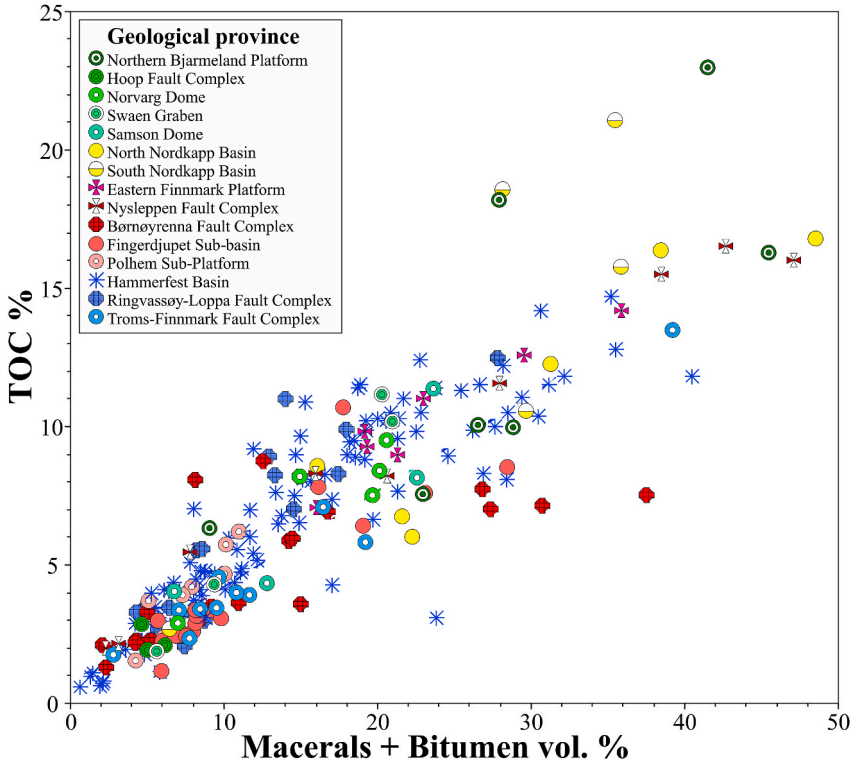

Fig. 5. Relationship between volume percentage of organic particles (i.e. macerals + bitumen) in whole rock versus total organic carbon (TOC) weight percent for each of the studied samples. Samples are color-coded based on geological provinces. (For interpretation of the references to color in this figure legend, the reader is referred to the Web version of this article.)

from the Ringvassøy-Loppa Fault Complex and the southernmost well in central Hammerfest does amorphinite predominates over alginite. Alge Member shales from areas of the Hammerfest Basin adjoining the Loppa High record an increased content of terrestrial liptinites (Figs. 3 and 7A). In this case, the land-derived liptinitic fraction has less sporinite and cutinite than in most other localities and consists predominantly of colonial alginite (Fig. 6E).

Rocks of the Krill Member in the Hammerfest Basin and the Ringvassøy-Loppa High and Nysleppen fault complexes record higher proportions of vitrinite and terrestrial liptinite relative to the underlying Alge Member (Figs. 7B and 9). This condition causes the westwards increase in marine particles observed in the Alge Member rocks of the Hammerfest Basin to be less pronounced and restricted to fewer central-western localities. Remarkably high vitrinite contents (i.e. $\geq$ 70 %) are also detected in some sites neighboring the Loppa High (Fig. 3).

4.2.3. Western areas: Bjørnøyrenna Fault Complex and Fingerdjupet Sub-basin

Marine-derived liptinites predominate over terrestrial macerals in the southern end of the Bjørnøyrenna Fault Complex, accounting for up to 70 % of the average maceral composition in the overlying Krill Member (Figs. 7 and 8A). The marine organic fraction is predominantly composed of granular and finely disseminated fluorescent amorphinite, opposite to the high alginite inputs detected in most of the Hammerfest Basin. Northwards, the overall character of the kerogen in the Alge Member changes substantially and terrestrial macerals make up to 70 % of the organic fraction in the boundary between the Bjørnøyrenna Fault Complex and the Polhem Sub-platform (Figs. 7A and 8B).

The composition of the organic matter within both members in the western sites of the Fingerdjupet Sub-basin is essentially the same (Fig. 7). Vitrinite predominates and makes up to 70 % of the organic matter fraction (Fig. 8C). The next most abundant maceral is inertinite. Only few terrestrial liptinites are found while marine liptinites are nearly absent. Liptinitic particles increase to nearly 50 % within the Krill Member in the eastern part of the sub-basin (Fig. 7B). Marine and terrestrial liptinites occur in approximately equal abundance.

4.3. Source rock generative potential

4.3.1. TOC and Rock-Eval pyrolysis

TOC data for the Hekkingen Formation shows values from 0.45 to 24 wt % (Fig. 5). The distribution of TOC in a 65 m Hekkingen core is displayed in Fig. 3 and demonstrates some of the stratigraphic attributes previously described. There is a sudden downwards increase in TOC to values $\geq$ 7 wt %, which is, in most cases, coincident with the top of the discussed GR deflection. TOC values between 8 and 12 wt % are predominant within the organically richer Alge Member. The fine-grained sediments in the Polhem Sub-platform (Fig. 8B) are an exception to this generalization because TOC contents are lower than 7 %, but biostratigraphically controlled ages confirm they were laid down during Alge times (i.e. Callovian to early Kimmeridgian; Costa and Davey, 1992; Smelror and Below, 1993).

Total organic carbon contents within the Krill Member are diminished relative to the underlying Alge Member but are still sufficiently high to be considered petroleum source rocks (i.e. $\geq$2 wt %; Zumberge et al., 2012, Figs. 7–10). Values between 2 and 5 wt % occur more often. Organic-rich intervals alternate with only modestly enriched intervals, revealing the oscillatory nature of organic carbon sedimentation within the Krill Member (Fig. 3). This attribute of the Krill Member reflects a more discrete distribution of the organic matter when compared to the more consistent distribution observed throughout the Alge Member. It is noteworthy to highlight that some wells, particularly in the southern areas of the Bjarmaland Platform (Fig. 1), were drilled in or adjacent to structural highs, some of which are known to have been topographically higher during sedimentation of the Hekkingen Formation. TOC and HI values recorded in these locations probably represent minimum values owning to a systematic decrease in organic matter sedimentation, poor preservation conditions, and selective preservation of hydrogen poor particles.

The generative potential of thermally immature samples (e.g. Tmax $<$435 °C) can be assessed based on the hydrogen index (HI). This parameter is the result of S2 divided by TOC (i.e. S2/TOC x 100). In Fig. 10, the majority of the HI values are in the range of 50 and 450 mgHC/gTOC, indicating that the kerogen within both members has comparable oil and gas generation capabilities.

4.3.2. Relationships between geochemical and petrographic data

Because of the high percentage of particles visible under the microscope (i.e. Fig. 5), the maceral composition is expected to be reflected by bulk geochemical parameters (i.e. TOC and HI). A diagram of HI as a function of the relative abundance of liptinites (marine + terrestrial) provides the basis for comparing geochemical and petrographic data. In Fig. 11, there seems to be an overall positive correlation between HI and increasing contents of liptinites. Alge Member samples from the eastern Finnmark Platform show higher HI values than other samples containing comparable amounts of liptinites (Fig. 11A). Accordingly, this area records some of the most oil prone source rocks (i.e. among immature samples) as defined by average HI values of 373 and 387 mg HC/g TOC (Fig. 7A), which are typically associated with Type II/III kerogens. Alge samples from the Polhem Sub-platform also display HI values that are slightly higher than other samples with compositionally similar kerogen assemblages. An average HI value of 328 mg HC/g TOC in well 7220/5-2 is indicative of type II-III kerogen in this area.

The highest average (i.e. per well) TOC levels, i.e. 13 %, are recorded for the Alge Member rocks at the boundary between the Bjarmeland Platform and the Nysleppen Fault Complex and in the Northern Bjarmeland Platform (Fig. 7; Table 1). Average HI values of 315 and 366 mg HC/g TOC were computed for these two areas, respectively, which suggests the presence of kerogen type II/III.

Some Alge samples in the Nordkapp Basin possess moderately high TOC levels paired with HI values that are lower than expected from the overall TOC-HI relationships in Fig. 10A. Such low HI values also seem to be inconsistent with the relatively high content of liptinites in these samples (Fig. 11A). This discrepancy can be interpreted as reflecting oxidation or bacterial reworking of the organic matter, or both, leading to the formation of hydrogen-lean type III kerogen, which are at best only gas-prone. Early generation is ruled out as a possible cause because of the low Tmax values of 410 °C measured in these samples (Table 1). The Alge and Krill members contain mostly a mixed type III/II kerogen (i.e. 200 to 300 mgHC/gTOC) across the southern Nordkapp Basin and the adjacent southern Bjarmeland Platform (i.e. Norvarg and Samson domes, Swaen Graben, Hoop Fault Complex). This only modest generative potential appears to be consistent with the predominance of terrestrial organic particles.

In the southern end of the Hammerfest Basin and in the adjacent Troms-Finnmark Fault Complex, both the Alge and Krill members have average HI values generally less than 200 mg HC/g TOC (Figs. 7 and 9A). This might have been anticipated because of the high concentrations of humic kerogen of a vitrinitic nature. Hydrogen-poor, type III kerogen also occurs within Krill Member sediments deposited in the northeastern corner of the Hammerfest Basin (i.e. average HI 190 mgHC/gTOC) and the neighboring Nysleppen Fault Complex (i.e. HI 191 mgHC/gTOC) (Fig. 7B). Along the eastern margin of the Hammerfest Basin, the Alge Member displays average TOC values ranging from 9 to 13 %; and the Krill Member shows lower average values ranging from 4 to 6 wt % (Fig. 7). The preferential accumulation of land-derived organic particles is reflected in only moderate HI values spanning from 260 to 280 mg HC/g TOC and from 287 to 321 mgHC/gTOC, respectively.

4.3.3. Estimations of initial generative potential in thermally mature areas

Hydrogen indices in the central and western areas of the Hammerfest

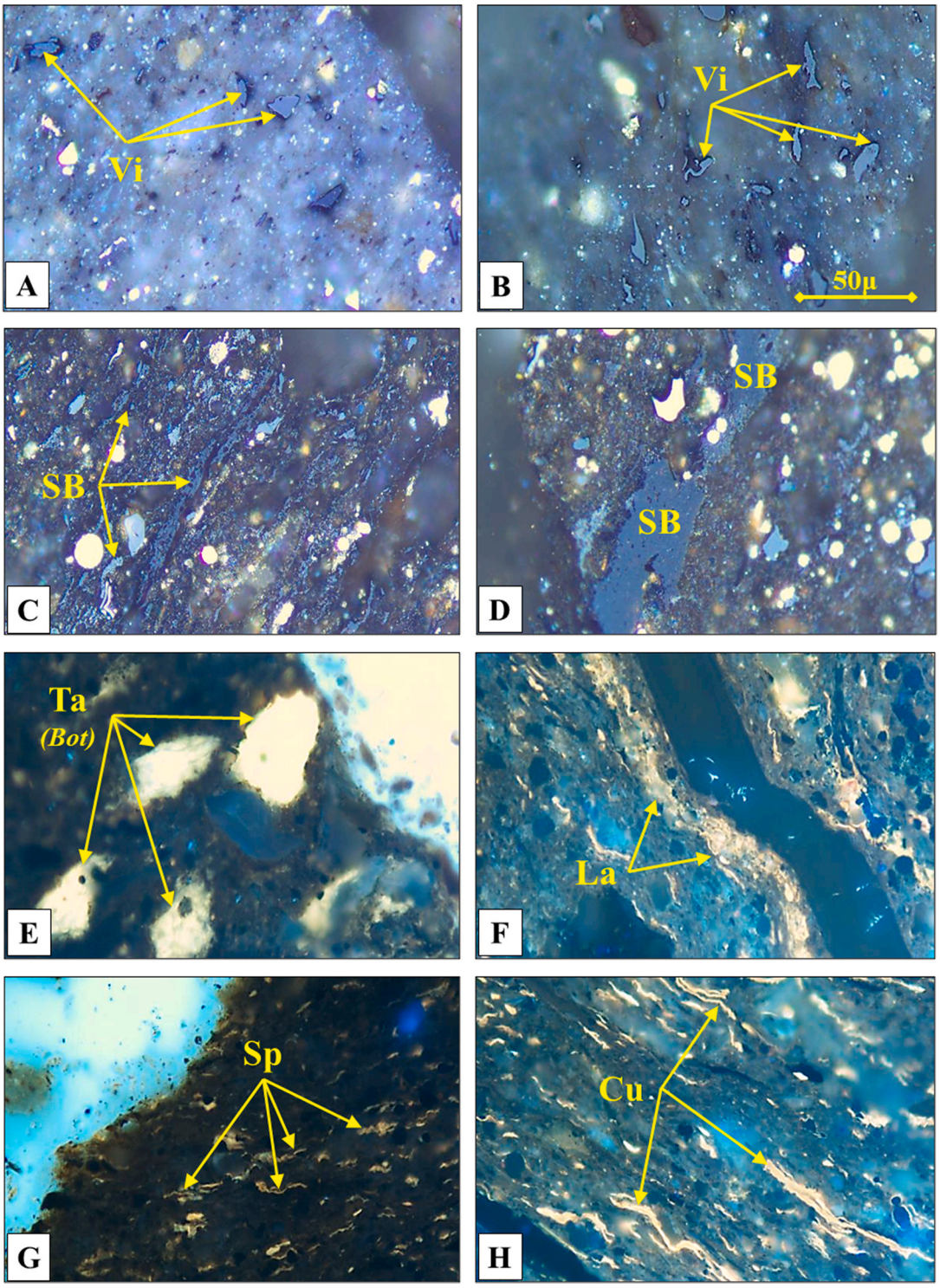

Fig. 6. Photomicrographs of representative maceral types in the dataset taken at 500X magnification. **A and B**. Photos in white-light of vitrinite maceral, and vitrodetrinite (Vi), within a mineral matrix mostly composed of quartz. Vitrodetrinite particles are those defined as being smaller than 10µ in size. Photo A: well 7120/1–2 at 1912m; Photo B: well 7119/12-1 at 2511 m. **C and D**. Photos in white-light of granular solid bitumen (SB) illustrating dark grey to light grey reflectance. Solid bitumen is differentiated from in-situ vitrinite by its granular appearance and generally lower reflectance (darker grey color). Photo C: well 7119/12-1 at 2595 m; Photo D. well 7120/2-2 at 2144 m. **E.** Photo in UV-light of telalginite maceral (Ta) in this instance Botryococcus-like colonial algae. Note the feathery edges of the colonial algae characteristic of this maceral. The bright yellow fluorescence indicates relatively low maturity. Well 7120/2-3 S at 2005.93 m. **F.** Photo in UV-light of lamalginite (La) illustrating the laminated nature of the fluorescing organic matter. Well 7120/2-3 S at 2005.93 m. **G:** Photo in UV-light of fluorescing sporinite (Sp). In these instances the fluorescing material is likely terrestrial pollen. Well 7120/2-3 S at 2005.93 m. **H.** Photo in UV-light of fluorescing material, most importantly cutinite (Cu) which are the fluorescing cuticles in terrestrial plant material. Note the abundant other fluorescing organic matter including sporinite (terrestrial pollen) and liptodetrinite (fluorescing organic matter smaller than 10µ in size). Well 7120/2-3 S at 2005.93 m. (For interpretation of the references to color in this figure legend, the reader is referred to the Web version of this article.)

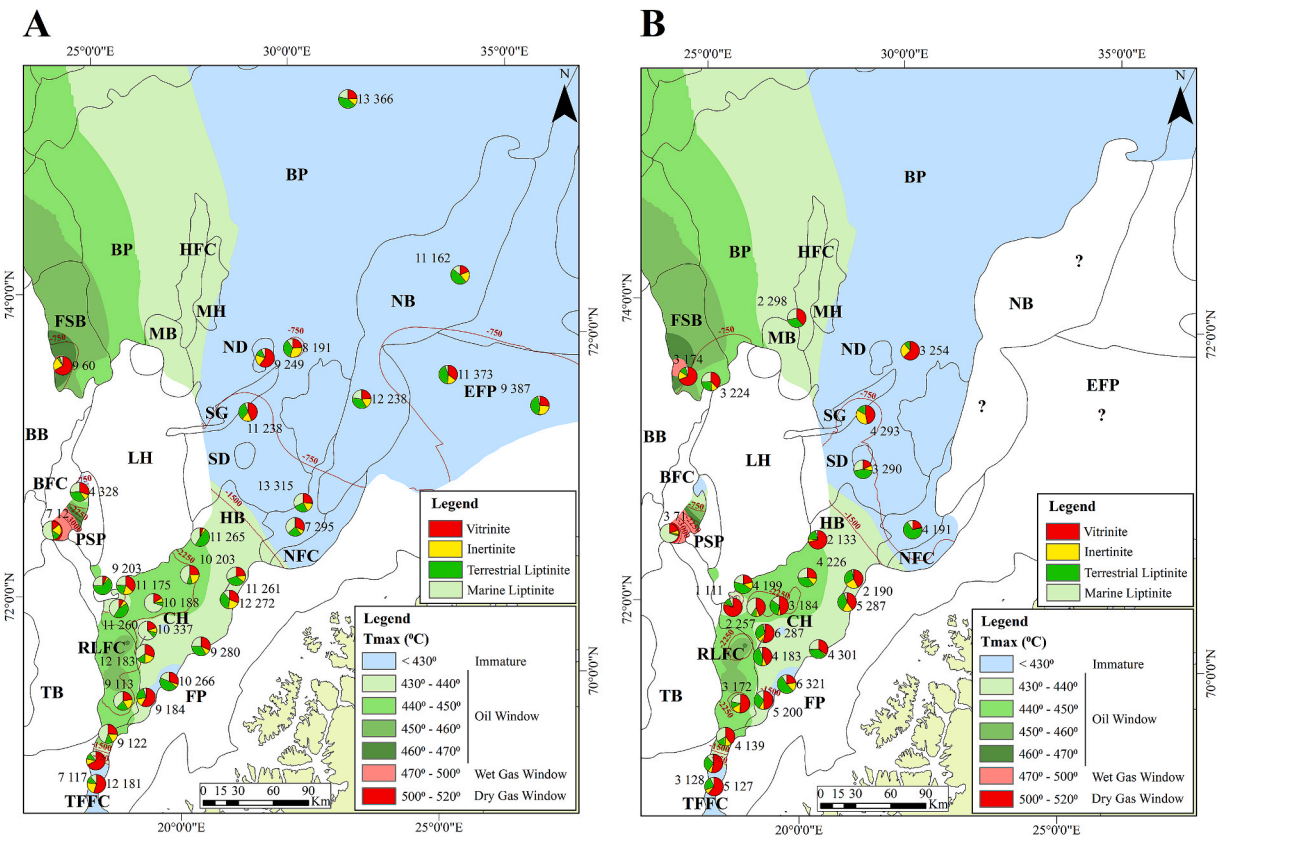

Fig. 7. Map of the southwestern Barents Sea illustrating the variability in maceral compositions within the Alge (**A**) and Krill (**B**) members. The pie diagrams represent the average (i.e. per well) maceral compositions calculated from the microscopic analysis. Accompanying labels represent the average (i.e. per well) total organic carbon (TOC) and hydrogen index (HI). A present-day maturity overlay of the Hekkingen Formation calculated from Tmax Rock-Eval data is also displayed. See Table 1 for plotted values. Refer to Fig. 1 for abbreviations of the different geological provinces.

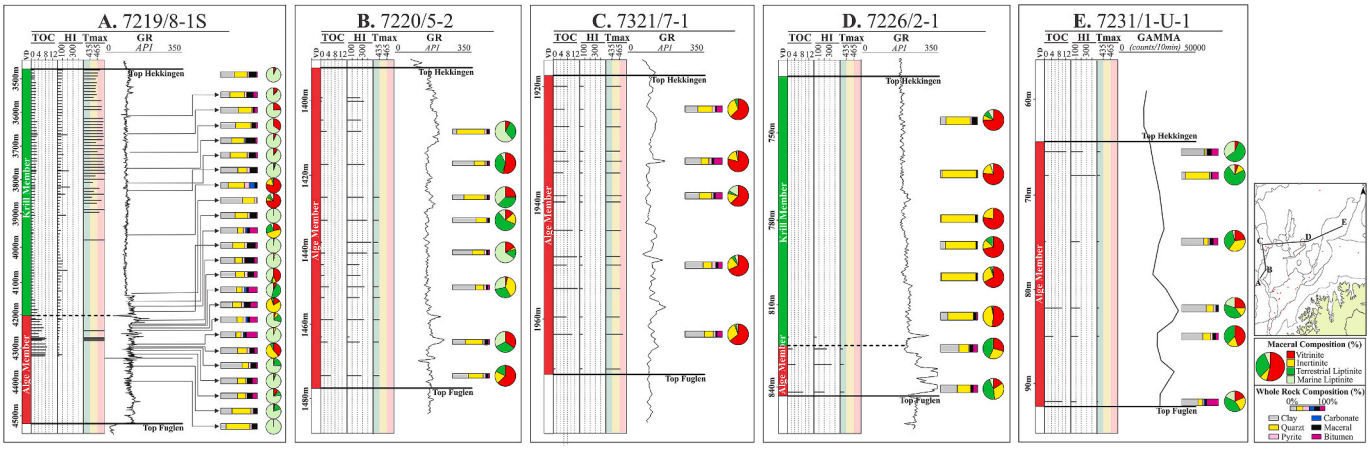

Fig. 8. Gamma ray (GR) logs, source rock geochemical data (i.e. TOC, HI, Tmax), and maceral and mineral composition of studied Hekkingen samples from different wells: **A.** 7219/8-1 S = Bjørnøyrenna Fault Complex; **B.** 7220/5-1 = Polhem Sub-platform; **C.** 7321/7-1 = Fingerdjupet Sub-basin; **D.** 7226/2-1 = Southern Bjarmeland Platform; **E.** 7231/1-U-1 = Nordkapp Basin. See inset map for well locations.

Basin, the Ringvassøy-Loppa and Bjørnøyrenna fault complexes, and the Fingerdjupet Sub-basin are diminished because of the marginal to mature nature of the Hekkingen Formation (Fig. 7). Thermal stress has probably led to different levels of hydrogen losses considering the thermal stability of the various maceral types. An average initial hydrogen richness (HIi) range is estimated by integrating observations from maceral composition and back-calculation. A HIi range is obtained empirically from comparing the HI of thermally mature samples with that of immature samples of similar maceral composition. A second range is calculated by translating the measured HI of mature samples along the maturation pathways on a Tmax versus HI cross-plot. Modestly elevated HIi values between 350 and 400 mg HC/g TOC are tentatively estimated for the marine liptinite rich kerogens within the Alge Member shales in the central Hammerfest Basin (i.e. Figs. 7 and 9C). Maceral assemblages made up of roughly equal proportions of marine and terrigenous liptinites in the Alge Member shales neighboring the Loppa High (i.e. Fig. 3) are assigned HIi values between 280 and 330 mgHC/gTOC. Lower HIi values between 250 and 300 mg HC/g TOC are

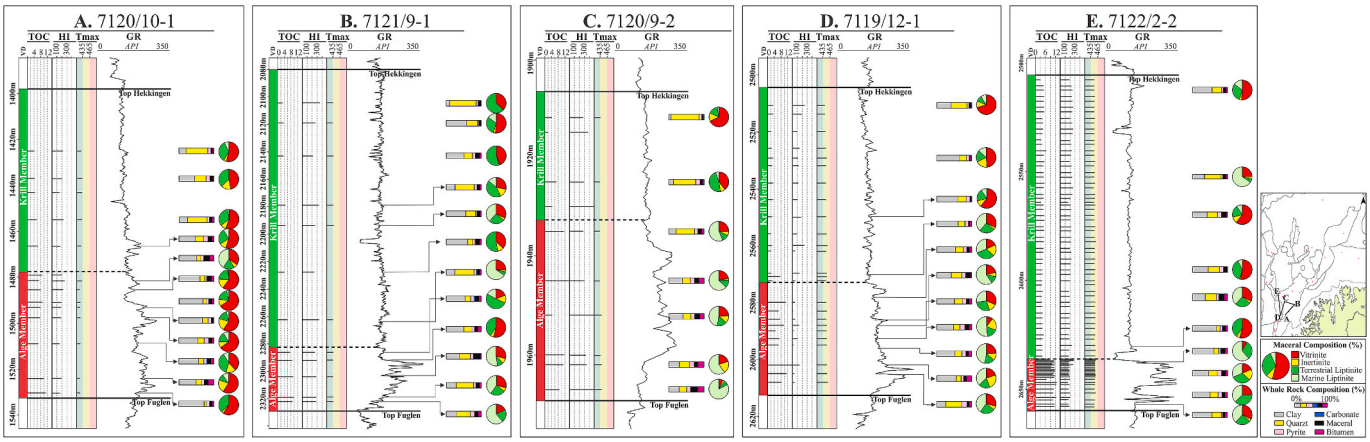

Fig. 9. Gamma ray (GR) logs, source rock geochemical data (i.e. TOC, HI, Tmax), and maceral and mineral composition of studied Hekkingen samples from different wells: A. 7120/10-1 = Southern Hammerfest Basin; B. 7121/9-1 = Eastern Hammerfest Basin. C. 7120/9-2 = Central Hammerfest Basin; D. 7119/12-1 = Ringvassøy-Loppa Fault Complex; E. 7122/2-2 = Western Hammerfest Basin. See inset map for well locations.

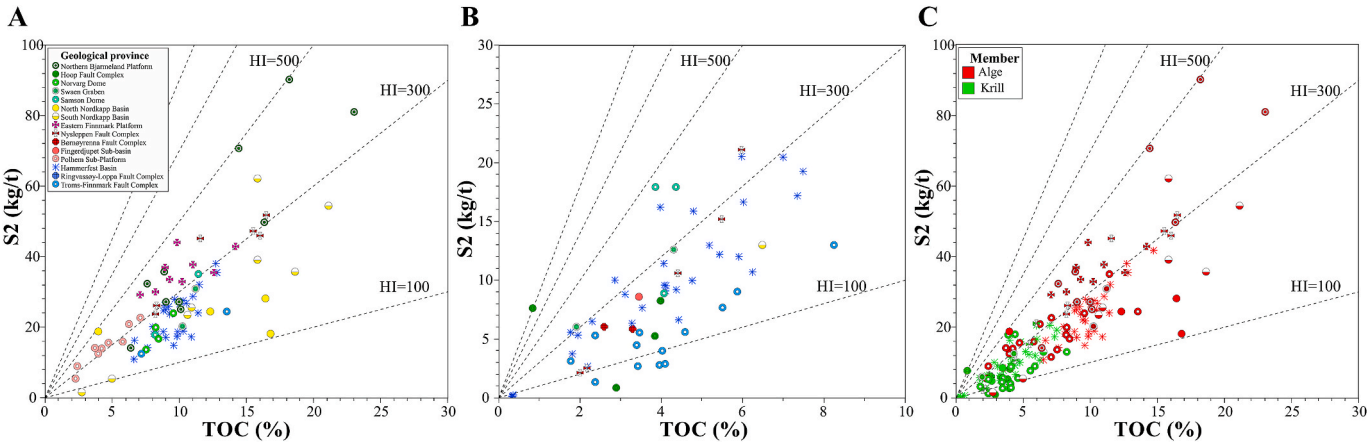

Fig. 10. Total organic carbon (TOC) versus Rock-Eval S2 peak (S2) cross-plot of thermally immature (i.e. < Tmax 430 °C) samples from the Alge (**A**) and Krill (**B**) members. **C**. Combined data from both members. Samples are color-coded based on geological provinces (i.e. A and B) or Hekkingen members (i.e. C). The complete dataset with Tmax values is displayed in Fig. 2. (For interpretation of the references to color in this figure legend, the reader is referred to the Web version of this article.)

estimated for the more terrestrially influenced kerogens within the overlying Krill Member (Fig. 9). Southwards into the Ringvassøy-Loppa Fault Complex, initial hydrogen richness is estimated to have been between 270 and 320 mg HC/g TOC for both members. As will be discussed in section 4.4, sedimentary organic matter in these areas, particularly within the Alge Member, is suspected to have been differentially affected by the action of sulfate-reducing bacteria. This condition may in turn have depressed the original hydrogen richness of the organic materials to different extends, leading to HIi lower than estimated.

Original HI values lower than 200 mg HC/g TOC are estimated for the vitrinitic kerogen in the western localities of the Fingerdjupet Subbasin (i.e. Figs. 7 and 8C) and some Krill sites in the west of the Hammerfest Basin (i.e. Fig. 3). The high quantities of oil-prone, fluorescent amorphous macerals in the Bjørnøyrenna Fault Complex (i.e. Fig. 8A) is indicative of accumulation of "authentic" marine type II kerogen containing elevated hydrogen indexes. Based on analog data from discrete, amorphinite-rich intervals documented in the Polhem sub-platform, a feasible prognosis of HIi for such maceral characteristics would be around 400–500 mgHC/gTOC, or even higher depending on syn- and post sedimentary alteration.

4.4. Sedimentary conditions during sedimentation

4.4.1. TOC versus pyrite

Under marine, oxygen-limited conditions, sulfate-reducing bacteria utilizes sulfate as their main source of oxygen (Berner, 1984). The reduced inorganic sulfide is largely fixed as pyrite (FeS_2) depending on the supply of both reactive iron and bacterially decomposable organic matter, which acts as both a reductant for sulfate and as an oxygen-consuming barrier that prompts anoxic conditions (Berner, 1984). This premise permits the relationship between sedimentary pyrite and TOC to be used as a qualitative tool to evaluate the redox state of the depositional environment (Berner and Raiswell, 1983; Leventhal, 1983; Berner, 1984). Fig. 12 compares samples from the Alge (A) and Krill (B) members in terms of TOC content (wt %) and volume percentage of pyrite from the microscopic analyses. TOC and pyrite correlate positively with one another for Krill samples (Fig. 12B). This is characteristic of sediments deposited in normal marine (i.e. moderately low oxygen content) bottom waters (Berner, 1984; Raiswell et al., 1988; Lückge et al., 2002). Under such conditions, dissolved sulfide and reactive detrital iron minerals are plentiful and, hence, the major control on pyrite formation is the available amount and reactivity of decomposable organic matter.

In the Alge samples, pyrite displays a weaker correlation with TOC

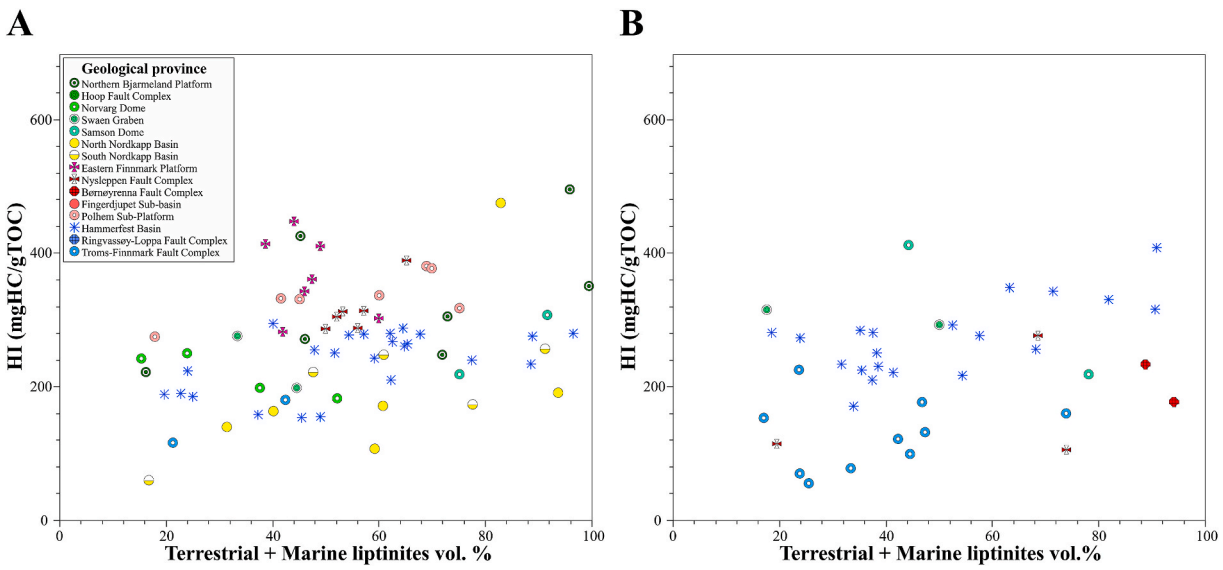

Fig. 11. Relationship between volume percentage of liptinitic macerals (i.e. marine + terrestrial liptinites) and hydrogen index (HI) of thermally immature (i.e. < Tmax 430 °C) samples from the Alge (**A**) and Krill (**B**) members. Samples are color-coded based on geological provinces. (For interpretation of the references to color in this figure legend, the reader is referred to the Web version of this article.)

and its concentration seems independent of TOC (Fig. 12A). This attribute of the Alge Member is typical of accumulation and burial of organics in anoxic settings (Berner, 1984). There, a plentiful supply of organic carbon and sulfide leads to the formation of high concentrations of pyrite, which is in this case limited by the amount of reactive iron-minerals and, importantly, time for reaction. Similar to the Krill Member, highest pyrite concentrations (up to 18 wt %) occur preferentially in samples from the most southernly located areas, i.e. Hammerfest Basin and Ringvassøy Fault Complex. Samples from other locations with comparable TOC levels exhibit a lower pyrite content. This possibly results from the coincidental development of relatively more anoxic bottom waters and stronger inputs of reactive iron minerals in the southern depositional sites. Under strongly anoxic conditions, sulfide occurs in the bottom water and in the upper few meters of the sediments (Sweeney and Kaplan, 1980; Berner, 1984) and even the slowly reacting iron compounds have sufficient time to react with high concentrations of sulfide (Leventhal, 1983).

4.4.2. *Carbon isotopes of the SARA fractions*

The carbon isotopic composition of the $\delta^{13}C$ saturate (C_{sat}), aromatic (C_{aro}) and asphaltene (C_{asp}) fractions (i.e. SARA) of the organic matter in sedimentary rocks is the result of the original composition of the organic precursors and secondary biochemical processes altering it during sedimentation and diagenesis (Macko et al., 1998; Hayes et al., 1999). The carbon isotope composition of the Hekkingen Formation undergoes a gradual northwards change from heaviest in the Ringvassøy Loppa-High Fault Complex/southern Hammerfest Basin to lightest in the northern Bjarmeland Platform (Fig. 13A and B).

In an attempt to elucidate the effects of organic matter type (i.e. marine versus terrestrial) in the isotope signature, the relative maceral composition and the SARA isotope fractions of the reactive portion of the kerogen are cross plotted in Fig. 14. The plotted SARA isotope values indicate that samples containing different proportions of terrestrial- and marine-derived organic matter have a relatively uniform range of values. This suggests that although the primary composition of the organic matter has the main imprint on the original isotope signature, secondary processes may have altered it to different degrees.

Bacterial sulfate reduction is a complex biochemical process that not only releases sulfide but also alters the original isotopic composition of the organic matter owning to the preferential consumption of light isotopes (Jørgensen, 1982; Berner, 1984). By applying this logic, higher concentrations of pyrite indicate increasingly anoxic conditions leading to intensified bacterial activity and stronger isotope alteration towards heavier values. Cross-plots of pyrite and isotopes show that Alge samples from the Ringvassøy-Loppa Fault Complex and from the Hammerfest Basin record the highest pyrite contents and the heaviest isotopic composition (Fig. 15A and C). This correlation satisfactorily supports that accumulation of organic rich sediments within these areas occurred under more anoxic and stronger sulfate-reducing conditions relative to other areas in the dataset. The smaller variability in the content of pyrite and isotope values observed in the Krill Member (Fig. 15B and D) implies that although redox conditions seemingly changed across the Barents Sea during its deposition, the zonation in dissolved oxygen levels were not as significant as in Alge times. It is arguable that thermal maturity has shifted the original isotope composition to heavier (i.e. less negative) values. In such case, the degree of thermally-induced alteration would vary according to the stability of the different kerogen types. Nevertheless, the magnitude of this changes is not expected to be significant given the only marginal to mid-thermal maturity (Fig. 7; Table 1) of the samples plotted in Fig. 15.

Doerner et al. (2020) have considered the implications of organic matter lability in isotope alteration caused by sulfate-reducing bacteria. Sediments containing higher amounts of labile organic matter were found to have experienced heavier degradation by sulfate reducers. Samples from the Ringvassøy-Loppa Fault Complex and the Hammerfest Basin record high concentrations of labile marine liptinites relative to other areas (Fig. 7). This condition may have eventually prompted a more extensive alteration of the original carbon isotopic composition and, importantly, diminished the original hydrogen richness.

5. Discussion: relationships between paleogeography, macerals, and source rock potential variations

5.1. *Sedimentation of the Alge Member*

The paleogeographic scenario for the Late Jurassic in the Norwegian Barents Sea is from Marin et al. (2020). They interpret the Hekkingen Formation as part of an overall transgressive event with minor superimposed transgressive-regressive movements. In their model, regional flooding of the shelf begins in the Bathonian-Oxfordian with deposition of the Fuglen Formation. Further transgression during the Oxfordian–Kimmeridgian caused terrigenous sediments to be trapped

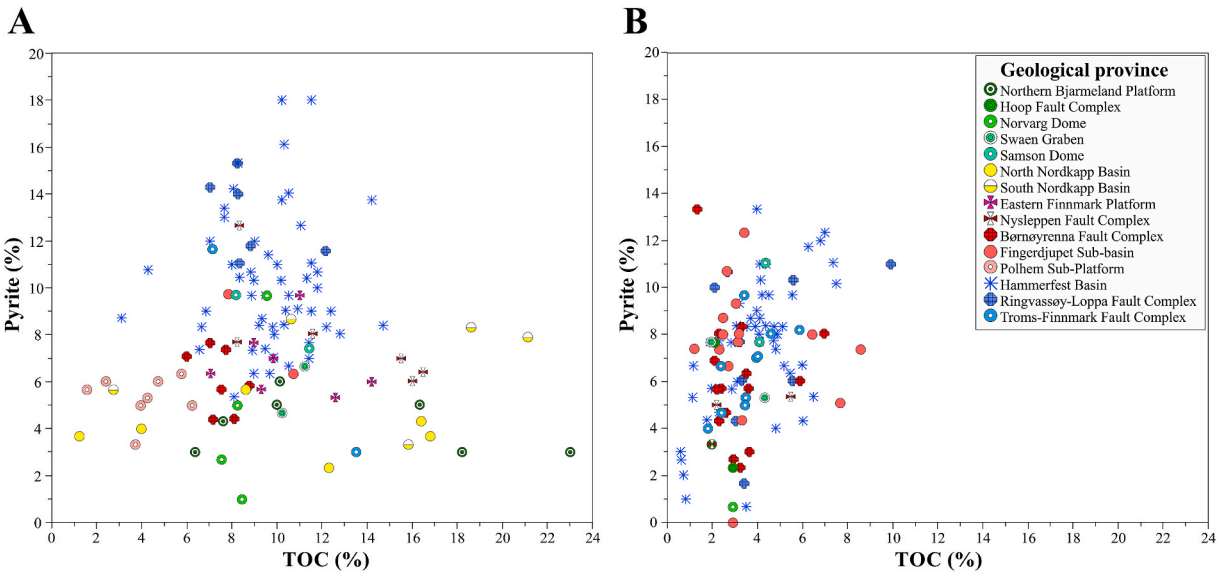

Fig. 12. Cross-plot of total organic carbon (TOC) weight percent versus whole rock volume percentage of pyrite (Pyrite %) for each of the samples from the Alge (**A**) and Krill (**B**) members. Samples are color-coded based on geological provinces. (For interpretation of the references to color in this figure legend, the reader is referred to the Web version of this article.)

landward with an associated drop in sedimentation rates farther offshore, marked by deposition of the black shales of the Alge Member. In the Hammerfest Basin and the Troms-Finnmark and Ringvassøy-Loppa fault complexes, outer shelf facies accumulated (Fig. 16A). This water mass transitioned westwards into the Tromsø Basin where cooler, deep marine facies were deposited. In these areas, a relatively high pyrite content and heavy isotopes (Fig. 15A) suggest a depositional environment with poorly oxygenated bottom waters. Under these conditions, intense degradation by sulfate-reducing bacteria is suspected to have decomposed the organic matter and probably depressed the HI values of preferentially algal debris (Littke et al., 1997; Luckge et al., 2002; Doerner et al., 2020). The westwards enrichment in marine organic components in the Hammerfest Basin reflects an increasing distance from the sources of land particles, which is inferred to be the Norwegian mainland.

The Loppa High remained under shallow water conditions and only uplifted footwall islands emerged above sea level (Fig. 16A). The higher content of colonial alginite recorded in the western Hammerfest Basin supports the existence of an inner shelf to transitional source area updip in the Loppa High. The isolated islands are likely sources for the abundant terrestrial organic matter in the Fingerdjupet Sub-basin, the Polhem Sub-platform, the Bjørnøyrenna Fault Complex, and the southern part of the Bjarmeland Platform. It is also possible that small islands established on top of the Samson and Norvarg domes and on top of uplifted footwalls around the Swaen Graben acted as additional sources of terrestrial debris in the southern Bjarmeland Platform.

Across most of the Nordkapp Basin, the Bjarmeland Platform, and the distal parts of the eastern Finnmark Platform, the Alge Member was deposited in an outer shelf setting with high inputs of terrestrial organic particles from the mainland and locally from islands formed on top of salt diapirs (Fig. 16A). In the Nordkapp Basin, marine liptinites possibly derived from autochthonous organisms living in semi-sealed mini basins formed between diapirs. Therein, the intermittent growth of salt diapirs (Rojo and Escalona, 2018; Cedeño et al., 2019) probably caused small-scale fluctuations in redox conditions and subjected the organic matter to reworking and degradation by aerobic bacteria, which consequently lowered HI (i.e. Fig. 10A) and increased the concentration of inertinite (i.e. Fig. 8E). Such fluctuations in dissolved oxygen content

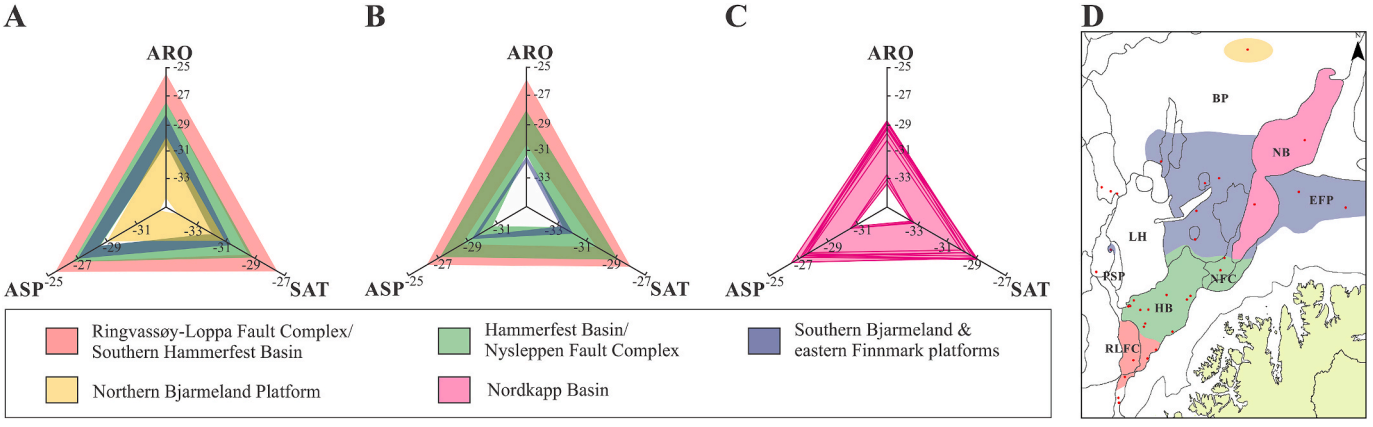

Fig. 13. North-south variability in carbon isotope composition within the Alge (**A**) and Krill (**B**) members. The isotope ranges displayed in the three-axes diagrams represent the minimum and maximum value for each of the SARA (Saturate, Aromatic, Asphaltene) fractions of samples in the corresponding region. **C.** Isotope ranges and samples of the Alge Member in the Nordkapp Basin are displayed. **D.** Map of the study area color-coded after the three-axes diagrams. Refer to Fig. 1 for abbreviations of the different geological provinces. (For interpretation of the references to color in this figure legend, the reader is referred to the Web version of this article.)

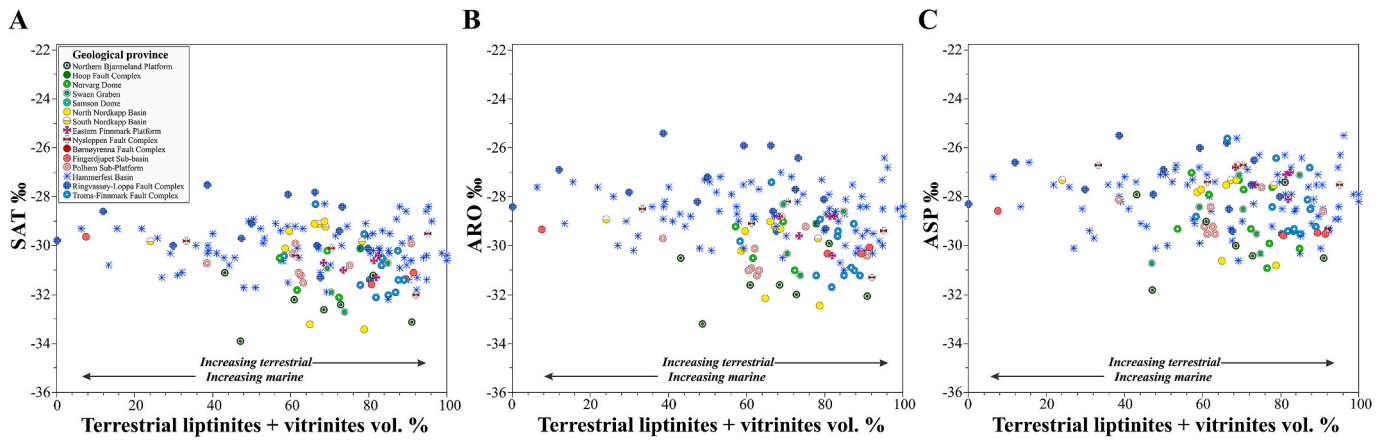

Fig. 14. Volume percentage of terrestrial macerals (i.e. vitrinite + terrestrial liptinites) cross-plotted versus isotope values of the saturate-SAT (**A**), aromatic-ARO (**B**), and asphaltenes-ASP (**C**) fractions of the studied source rock samples. Samples are color-coded based on geological provinces. (For interpretation of the references to color in this figure legend, the reader is referred to the Web version of this article.)

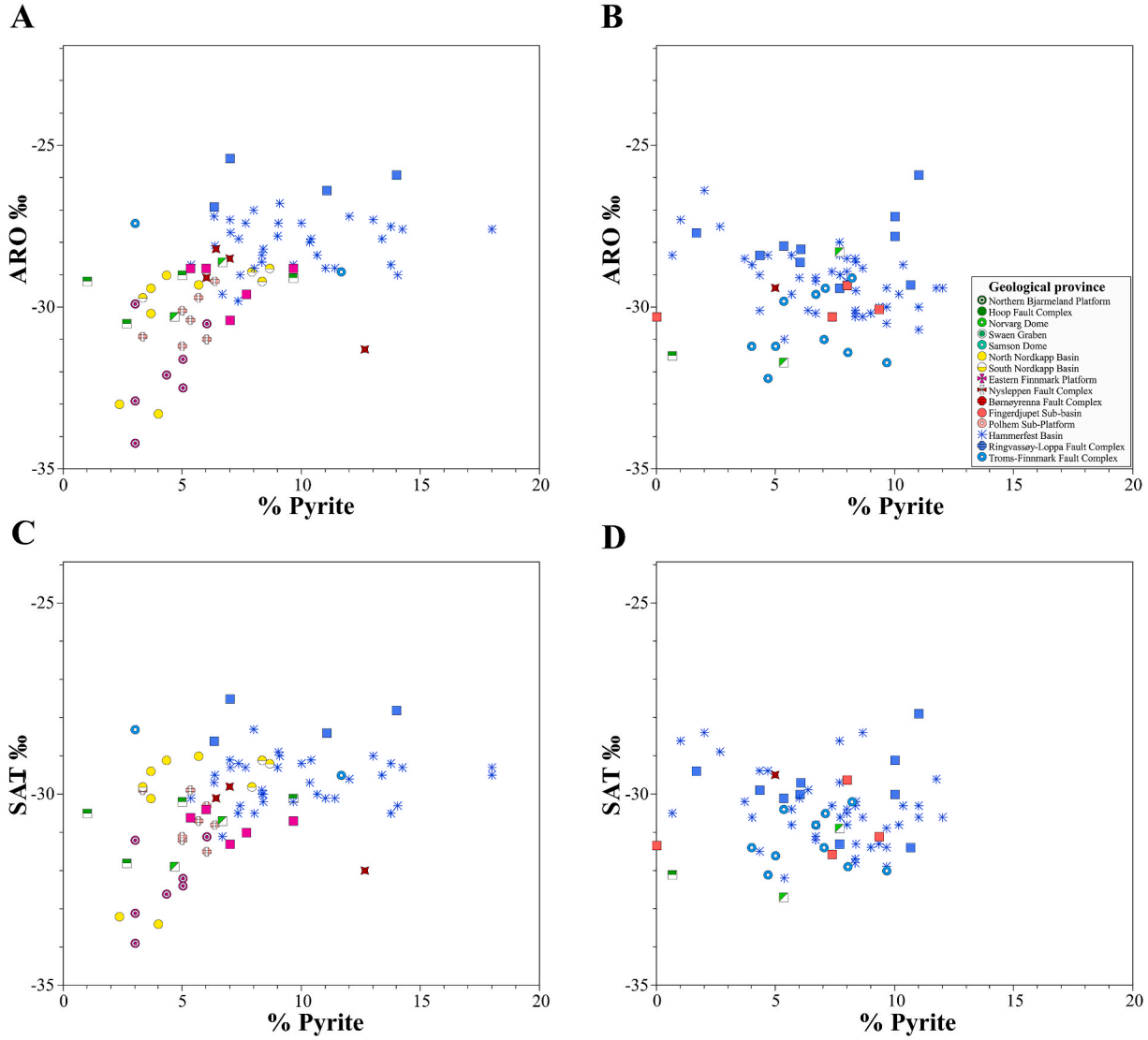

Fig. 15. Cross-plot of whole rock volume percentage of pyrite (Pyrite %) versus isotope values of the saturate (SAT) and aromatic (ARO) fractions of source rock from the Alge (**A** and **C**) and Krill (**B** and **D**) members, respectively. Samples are color-coded based on geological provinces. (For interpretation of the references to color in this figure legend, the reader is referred to the Web version of this article.)

in the Nordkapp Basin are probably responsible for the broad range of isotope values covering a span of up to 4.3‰ (Fig. 13C). Higher-than-average HI values in the eastern Finnmark, the northern Bjarmeland, and the Polhem Sub-platforms may be a result of less degradation by sulfate reducers under only modestly anoxic conditions. Lighter isotopes and lower contents of pyrite compared to the Hammerfest Basin and the Ringvassøy Fault Complex (Fig. 15A) suggest affinities with less anoxic bottom waters in the northern areas.

5.2. Sedimentation of the Krill Member

Increased tectonic activity during the late Kimmeridgian–Ryazanian brought about paleogeographic changes (Fig. 16B) that exerted important controls on the sedimentation of the Krill Member. Seawards migration of the shorelines and subaerial erosion of uplifted footwalls delivered higher volumes of coarse-grained sediments to the shelf, which locally increased sedimentation rates and diluted the organic matter. The generally coarse grain size of the clastic particles and the increased freshwater discharge imply a more energetic hydraulic regimen and greater contents of dissolved oxygen. This sedimentary background resulted in accumulation of the Krill Member under redox conditions that were generally more uniform across the different geological provinces compared to the accumulation during Alge times. Importantly, the biota sourcing the sedimentary organic matter remained essentially the same as in the underlying Alge Member, as discussed in section 4.2.

A set of normal faults caused further deepening of the shelf across the Ringvassøy-Loppa Fault Complex and development of deep marine environments (Fig. 16B). Most of the contiguous Hammerfest Basin remained under outer shelf conditions except for the Central High, which rose above sea level and shed terrestrial organic materials into the basin. Faulting along the Troms-Finnmark Fault Complex triggered the exhumation of the Finnmark Platform, followed by seaward migration of the shoreline and increased river runoff. Naturally, this caused the amount of terrestrial clastic and organic material delivered to the Hammerfest Basin and other areas adjacent to the Finnmark Platform to increase when compared to the underlying Alge Member (Fig. 16B). Sediments derived from the Norwegian mainland were probably deposited in delta and prodelta environments and were subsequently dispersed by turbiditic currents and hyperpycnal flows. Fewer inertinitic particles in the Hammerfest Basin and the Troms-Finnmark Fault Complex suggests short residence time in areas of oxic decomposition and supports the proximity of the continental source. Limited sulfate-reducing activity together with strong inputs of terrestrial organic matter, which is less susceptible to the attack by sulfate reducers, most likely prevented extensive decomposition of the organic matter and better preservation of the original hydrogen richness.

The Loppa High continued to be a tectonically active area and uplifted footwall islands became areally more extensive during Krill times (Fig. 16B). Shallow, inner shelf conditions existing in the Loppa High extended eastwards into the southern Bjarmeland Platform, the Nordkapp Basin, and the eastern Finnmark Platform. There, organic matter resided a longer time in the oxygenated uppermost sediment layer after deposition, where aerobic bacteria and bottom-dwelling fauna degraded all but the most resistant organic constituents. This lends itself to explaining a subtle increase in inertinite particles on the platforms, and possibly explains the lack of marine macerals.

5.3. Sedimentation within the Bjørnøyrenna Fault Complex

Subaqueous and subaerial degradation of uplifted footwalls in the Loppa High delivered increased volumes of clastic material to deep

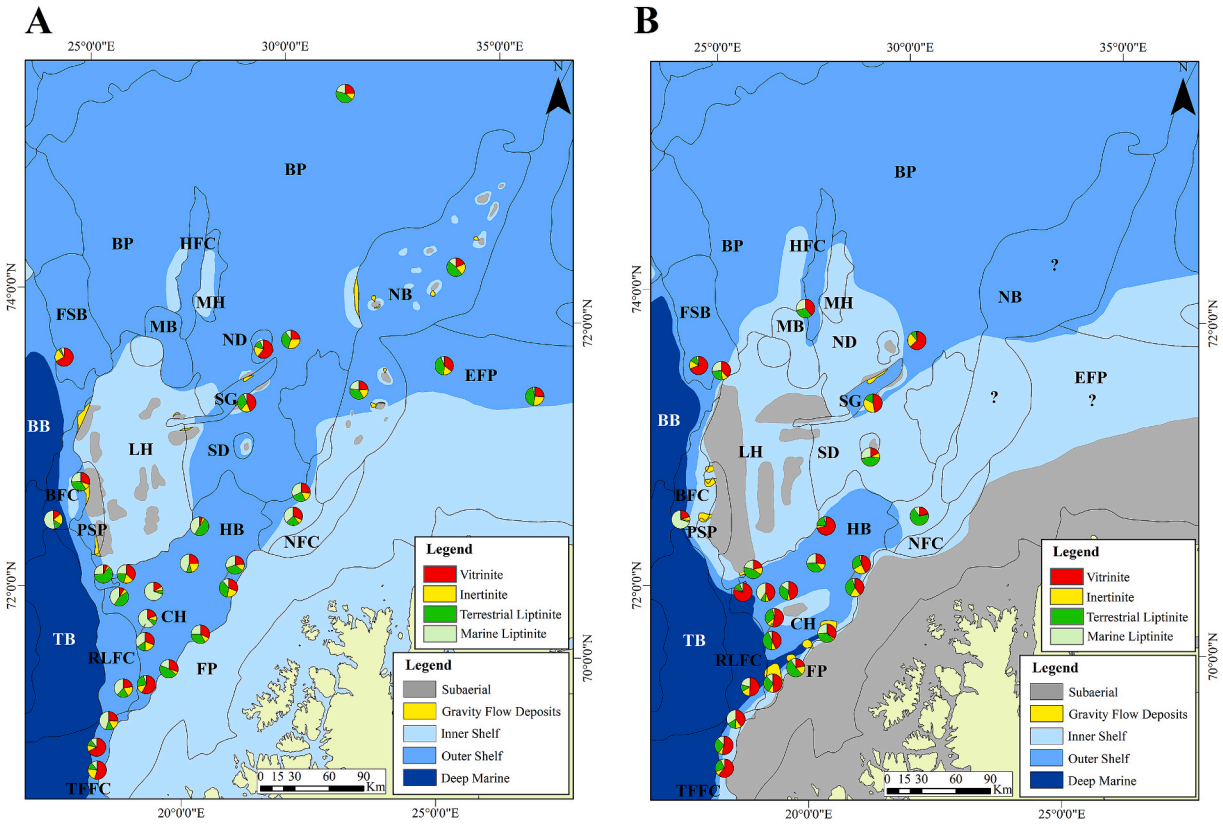

Fig. 16. Paleogeographic maps of the southwestern Barents Sea illustrating the variability in sedimentary environments within the Alge (**A**) and Krill (**B**) members. The paleogeographic maps are modified from Marin et al., (2020). The pie diagrams represent the average (i.e. per well) maceral compositions calculated from the microscopic analysis. See Table 1 for plotted values. Refer to Fig. 1 for abbreviations of geological provinces.

marine settings in the Bjørnøyrenna Fault Complex (Fig. 16B). Fig. 8A shows variability in organic facies reflected in shifts from high relative amounts of marine macerals (i.e. amorphinite) to high amounts of allochthonous terrestrial macerals (i.e. inertinite and vitrinite) within both members. This condition is consistent with short-lived, but frequent, changes in organic inputs and depositional conditions probably driven by submarine debris flows and turbiditic currents. These phenomena carried oxygenated waters and land plant-derived particles from proximal updip locations to deep sites where they disrupted the sedimentation of marine organic materials in oxygen-depleted waters. Oscillation in the concentration of pyrite and detrital quartz supports these interpretations (Figs. 12 and 8A). In this area of the Bjørnøyrenna Fault Complex, high sedimentation rates probably prevented oxidation and bacterial decomposition of the organic matter at the sediment-water interface.

6. Conclusions

The gross kerogen composition of the Hekkingen Formation is dominated by terrestrial organic matter. This conclusion arises from finding that vitrinitic and terrestrial liptinitic macerals predominate over marine macerals. Such preponderance of land-derived particles is more pronounced in the overlying Krill Member.

The abundance of marine macerals is higher in the central and western areas of the Hammerfest Basin and in well 7219/8-1 S in the Bjørnøyrenna Fault Complex. This suggests that authentic marine type II kerogens (i.e. $\leq$ 400 mgHC/gTOC) probably existed in these areas prior to thermal maturation.

The mapped shifts in the relative proportion of marine and allochthonous terrestrial macerals are ascribed to changes in the location of the depositional sites with respect to the sources of the terrestrial organic materials.

The highest levels of TOC ($\geq$7 wt %t) occur within the Alge Member, but the more discrete and organically poorer beds of the Krill Member still contain sufficient organic carbon to be classified as petroleum source rocks ($\geq$2 wt %).

Hydrogen indices between 50 and 400 mg HC/g TOC recorded throughout the entire formation indicate that both members have similar oil and gas generation capabilities. These HI values are characteristic of immature Type III to II-III kerogens and are generally consistent with the relatively high quantities of land-derived particles documented in this study.

Pyrite contents and carbon isotopes of the SARA fractions suggest that the degree of anoxia and bacterial sulfate reduction decreased gradually from south (i.e. Ringvassøy-Loppa Fault Complex/southern Hammerfest Basin) to north (i.e. Bjarmeland Platform). This zonation in redox conditions is more prominent in the Alge Member.

At least three factors controlled the detected variability in geochemical parameters: dilution rates of organic matter, varying proportions of terrestrial and marine organic particles, and the degree of preservation of the organic matter.

Declaration of competing interest

The authors declare that they have no known competing financial interests or personal relationships that could have appeared to influence the work reported in this paper.

Acknowledgments

The authors would like to thank the sponsors of the JuLoCrA project (https://wp.ux.uis.no/julocra/) for providing essential economic support. We are grateful to Integrated Geochemical Interpretation (IGI) for free software supply and to Applied Petroleum Technologies (APT) for analytical studies, especially to Per Erling Johansen. We sincerely thank the Norwegian Petroleum Directorate for providing sample material necessary to develop this research. The authors also thank reviewers Simon George, Dag Arild Karlsen, and Torbjørn Throndsen for their constructive reviews that greatly improved the manuscript.

References

Abay, T.B., Karlsen, D.A., Pedersen, J.H., Olaussen, S., Backer-Owe, K., 2017. Thermal maturity, hydrocarbon potential and kerogen type of some Triassic-Lower Cretaceous sediments from the SW Barents Sea and Svalbard. Petrol. Geosci. 24, 349–373. https://doi.org/10.1144/petgeo2017-035.

Århus, N., 1991. The transition from deposition of condensed carbonates to dark claystones in the Lower Cretaceous succession of the southwestern Barents Sea. Nor. Geol. Tidsskr. 71, 259–263.

Berglund, L., Augustson, J., Færseth, R., Gjelberg, J., Ramberg-Moe, H., 1986. The evolution of the Hammerfest Basin. Habitat of hydrocarbons on the Norwegian continental shelf 319–338.

Berner, R.A., Raiswell, R., 1983. Burial of organic carbon and pyrite sulfur in sediments over Phanerozoic time: a new theory. Geochem. Cosmochim. Acta 47, 855–862. https://doi.org/10.1016/0016-7037(83)90151-5.

Berner, R.A., 1984. Sedimentary pyrite formation: an update. Geochem. Cosmochim. Acta 48, 605–615. https://doi.org/10.1016/0016-7037(84)90089-9.

Berner, R.A., Kothavala, Z., 2001. GEOCARB III: a revised model of atmospheric CO2 over Phanerozoic time. Am. J. Sci. 301, 182–204.

Bjorøy, M., Hall, P.B., 1983. A rich Middle Triassic source rock in the Barents Sea area. In: Cheng, T.Y., Johnson, O.G. (Eds.), 3D Vector Forward Modeling – Proceedings of the 15th Annual Offshore Technology Conference. Society of Petroleum Engineers, Houston, Texas, pp. 379–392. https://doi.org/10.4043/4623-MS.

Blaich, O.A., Tsikalas, F., Faleide, J.I., 2017. New insights into the tectono-stratigraphic evolution of the southern Stappen high and its transition to Bjørnøya Basin, SW Barents Sea. Mar. Petrol. Geol. 85, 89–105. https://doi.org/10.1016/j.marpetgeo.2017.04.015.

Bugge, T., Elvebakk, G., Fanavoll, S., Mangerud, G., Smelror, M., Weiss, H.M., Gjelberg, J., Kristensen, S.E., Nilsen, K., 2002. Shallow stratigraphic drilling applied in hydrocarbon exploration of the Nordkapp Basin, Barents Sea. Mar. Petrol. Geol. 19, 13–37. https://doi.org/10.1016/S0264-8172(01)00051-4.

Cavanagh, A.J., Di Primio, R., Scheck-Wenderoth, M., Horsfield, B., 2006. Severity and timing of cenozoic exhumation in the southwestern Barents Sea. J. Geol. Soc. 163, 761–774. https://doi.org/10.1144/0016-76492005-146.

Cedeño, A., Rojo, L.A., Cardozo, N., Centeno, L., Escalona, A., 2019. The impact of salt tectonics on the thermal evolution and the petroleum system of confined rift basins: insights from basin modeling of the Nordkapp Basin, Norwegian Barents Sea. Geosciences 9. https://doi.org/10.3390/geosciences9070316.

Cedeño, A., Ohm, S., Escalona, A., Marín, D., Olaussen, S., Demchuck, T., 2021. SUBMITTED ALONG WITH THIS MS). Upper Cretaceous Source Rocks in the Norwegian Barents Sea, Part II: Insights from Open- and Closed-System Pyrolysis Experiments.

Clark, S., Glorstad-Clark, E., Faleide, J., Schmid, D., Hartz, E., Fjeldskaar, W., 2014. Southwest Barents Sea rift basin evolution: comparing results from backstripping and time-forward modelling. Basin Res. 26, 550–566. https://doi.org/10.1111/bre.12039.

Cornford, C., 1998. Source rocks and hydrocarbons of the north sea. In: Glennie, K.W. (Ed.), Petroleum Geology of the North Sea. Blackwell Science, Oxford, pp. 376–462. https://doi.org/10.1002/9781444313413.ch11.

Costa, L.I., Davey, R.J., 1992. Dinoflagellate cysts of the Cretaceous system. In: Powell, A.J. (Ed.), A Stratigraphic Index of Dinoflagellate Cysts. Chapman and Hall, London, pp. 99–131.

Dalland, A., Worsley, D., Ofstad, K., 1988. A lithostratigraphic scheme for the Mesozoic and Cenozoic succession offshore Norway north of 62 N. Norwegian Petrol. Dir. Bull. 4, 67.

Doerner, M., Berner, U., Erdmann, M., Barth, T., 2020. Geochemical characterization of the depositional environment of paleocene and eocene sediments of the tertiary central basin of Svalbard. Chem. Geol. 542 https://doi.org/10.1016/j.chemgeo.2020.119587.

Doré, A.G., Scotchman, I.C., Corcoran, D., 2000. Cenozoic exhumation and prediction of the hydrocarbon system on the NW European margin. J. Geochem. Explor. 69 (70), 615–618. https://doi.org/10.1016/S0375-6742(00)00137-0.

Dypvik, H., Mørk, A., Smelror, M., Sandbakken, P.T., Tsikalas, F., Vigran, J.O., Bremer, G.M.A., Nagy, J., Gabrielsen, R.H., Faleide, J.I., 2004. Impact breccia and ejecta from the Mjölnir crater in the Barents Sea-the Ragnarok Formation and Sindre bed. Norsk Geologisk Forening 84, 143–167.

Faleide, J.I., Gudlaugsson, S.T., Jacquart, G., 1984. Evolution of the western Barents Sea. Mar. Petrol. Geol. 1, 123–150. https://doi.org/10.1016/0264-8172(84)90082-5.

Faleide, J.I., Vågnes, E., Gudlaugsson, S.T., 1993. Late Mesozoic-Cenozoic evolution of the south-western Barents Sea in a regional rift-shear tectonic setting. Mar. Petrol. Geol. 10, 186–214. https://doi.org/10.1016/0264-8172(93)90104-Z.

Faleide, T.S., Midtkandal, I., Planke, S., Corseri, R., Faleide, J.I., Serck, C.S., Nystuen, J.P., 2019. Characterization and development of Early Cretaceous shelf platform deposition and faulting in the Hoop area, southwestern Barents Sea-constrained by high-resolution seismic data. Norw. J. Geol. 99, 3. https://doi.org/10.17850/njg99-3-7.

Gavshin, V.M., Zakharov, V.A., 1996. Geochemistry of the upper Jurassic - lower cretaceous Bazhenov Formation, West Siberia. Econ. Geol. 91, 122–133. https://doi.org/10.2113/gsecongeo.91.1.122.

Georgiev, S.V., Stein, H.J., Hannah, J.L., Xu, G.P., Bingen, B., Weiss, H.M., 2017. Timing, duration, and causes for late Jurassic-early cretaceous anoxia in the Barents Sea. Earth Planet Sci. Lett. 461, 151–162. https://doi.org/10.1016/j.epsl.2016.12.035.

Gernigon, L., Brönner, M., Roberts, D., Olesen, O., Nasuti, A., Yamasaki, T., 2014. Crustal and basin evolution of the southwestern Barents Sea: from Caledonian orogeny to continental breakup. Tectonics 33, 347–373. https://doi.org/10.1002/2013TC003439.

Grace, J.D., Hart, G.F., 1986. Giant gas fields of northern West Siberia. AAPG (Am. Assoc. Pet. Geol.) Bull. 70, 830–852. https://doi.org/10.1306/94886358-1704-11D7-8645000102C1865D.

Gudlaugsson, S.T., 1993. Large impact crater in the Barents Sea, 2 Geology 21, 291–294. https://doi.org/10.1130/0091-7613(1993)021<0291:LICITB>2.3.CO.

Hayes, J.M., Strauss, H., Kaufman, A.J., 1999. The abundance of 13C in marine organic matter and isotopic fractionation in the global biogeochemical cycle of carbon during the past 800 Ma. Chem. Geol. 161, 103–125. https://doi.org/10.1016/S0009-2541(99)00083-2.

Helleren, S., Marín, D., Ohm, S., Augustsson, C., Escalona, A., 2020. Why does not lithology correlate with gamma-ray spikes in the shaley source rocks of the Upper Jurassic Alge Member (southwestern Barents Sea)? Mar. Petrol. Geol. 121 https://doi.org/10.1016/j.marpetgeo.2020.104623.

Henriksen, E., Ryseth, A., Larssen, G., Heide, T., Rønning, K., Sollid, K., Stoupakova, A., 2011a. Tectonostratigraphy of the greater Barents Sea: implications for petroleum systems. In: Spencer, A.M., Embry, A.F., Gautier, D.L., Stoupakova, A.V., Sørensen, K. (Eds.), Arctic Petroleum Geology, vol. 35. Geological Society, pp. 163–195. https://doi.org/10.1144/M35.10. London, Memoirs 2011.

Henriksen, E., Bjørnseth, H.M., Hals, T.K., Heide, T., Kiryukhina, T., Kløvjan, O.S., Larssen, G.B., 2011b. Uplift and erosion of the greater Barents Sea: impact on prospectivity and petroleum systems. In: Spencer, A.M., Embry, A.F., Gautier, D.L., Stoupakova, A.V., Sørensen, K. (Eds.), Arctic Petroleum Geology, vol. 35. Geological Society, pp. 271–281. https://doi.org/10.1144/M35.17. London, Memoirs 2011.

Indrevær, K., Gabrielsen, R.H., Faleide, J.I., 2017. Early Cretaceous synrift uplift and tectonic inversion in the Loppa High area, southwestern Barents Sea, Norwegian shelf. J. Geol. Soc. 174, 242–254. https://doi.org/10.1144/jgs2016-066.

Johansen, S.E., Ostisty, B.K., Birkeland, Ø., Fedorovsky, Y.F., Martirosjan, V.N., Bruun Christensen, O., Cheredeev, S.I., Ignatenko, E.A., Margulis, L.S., 1992. Hydrocarbon potential in the Barents Sea region: play distribution and potential. In: Vorren, T.O., Bergsager, E., Dahl-Stamnes, Ø.A., Holter, E., Johansen, B., Lie, E., Lund, T.B. (Eds.), Arctic Geology and Petroleum Potential, vol. 2. Norwegian Petroleum Society, Special Publication, pp. 273–320. https://doi.org/10.1016/B978-0-444-88943-0.50024-1.

Jørgensen, B.B., 1982. Mineralization of organic matter in the seabed - the role of sulphate reduction. Nature 296, 643–645.

Kairanov, B., Marín, D., Escalona, A., Cardozo, N., 2019. Growth and linkage of a Basin-bounding fault system: insights from the early cretaceous evolution of the northern Polhem Subplatform, SW Barents Sea. J. Struct. Geol. 124, 182–196. https://doi.org/10.1016/j.jsg.2019.04.014.

Kairanov, B., Escalona, A., Norton, I., Abrahamsson, P., 2021. Early cretaceous evolution of the Tromsø Basin, SW Barents Sea. Mar. Petrol. Geol. 123 https://doi.org/10.1016/j.marpetgeo.2020.104714.

Klemme, H.D., 1994. Petroleum systems of the world involving Upper Jurassic source rocks. In: Magoon, L.B., Dow, W.G. (Eds.), The Petroleum System: from Source to Trap, vol. 60. AAPG Memoir, pp. 51–72.

Knies, J., Matthiessen, J., Christoph, V., Laberg, J.S., Hjelstuen, B.O., Smelror, M., Larsen, E., Andreassen, K., Eidvin, T., Vorren, T.O., 2009. The Plio-Pleistocene glaciation of the Barents Sea–Svalbard region: a new model based on revised chronostratigraphy. Quat. Sci. Rev. 28, 812–829. https://doi.org/10.1016/j.quascirev.2008.12.002.

Leith, T., Weiss, H., Mørk, A., Elvebakk, G., Embry, A., Brooks, P., Verba, M., 1993. Mesozoic hydrocarbon source-rocks of the Arctic region. In: Vorren, T.O., Bergsager, E., Dahl-Stamnes, Ø.A., Holter, E., Johansen, B., Lie, E., Lund, T.B. (Eds.), Norwegian Petroleum Society Special Publications, vol. 2. Elsevier, pp. 1–25. https://doi.org/10.1016/B978-0-444-88943-0.50006-X.

Leventhal, J.S., 1983. An interpretation of carbon and sulfur relationships in Black Sea sediments as indicators of environments of deposition. Geochem. Cosmochim. Acta 47, 133–137. https://doi.org/10.1016/0016-7037(83)90097-2.

Littke, R., Luckge, A., Welte, D.H., 1997. Quantification of organic matter degradation by microbial sulphate reduction for Quaternary sediments from the northern Arabian Sea. Naturwissenschaften 84, 312–315. https://doi.org/10.1007/s001140050402.

Luckge, A., Horsfield, B., Littke, R., Scheeder, G., 2002. Organic matter preservation and sulfur uptake in sediments from the continental margin off Pakistan. Org. Geochem. 33, 477–488. https://doi.org/10.1016/S0146-6380(01)00171-1.

Macko, S.A., Engel, M.H., Freeman, K., 1998. Variability of isotope compositions in modern and fossil organic matter. Chem. Geol. 152, 1–2.

Marín, D., Escalona, A., Grundvåg, S.A., Olaussen, S., Sandvik, S., Śliwińska, K.K., 2018. Unravelling key controls on the rift climax to post-rift fill of marine rift basins: insights from 3D seismic analysis of the Lower Cretaceous of the Hammerfest Basin, SW Barents Sea. Basin Res. 30, 587–612. https://doi.org/10.1111/bre.12266.

Marín, D., Helleren, S., Escalona, A., Olaussen, S., Cedeño, A., Nøhr-Hansen, H., Ohm, S., 2020. The Middle Jurassic to lowermost Cretaceous in the SW Barents Sea: interplay between tectonics, coarse-grained sediment supply and organic matter preservation. Basin Res. https://doi.org/10.1111/bre.12504.

Mørk, A., Dallmann, W., Dypvik, H., Johannessen, E., Larssen, G., Nagy, J., Nøttvedt, A., Olaussen, S., Pchelina, T., Worsley, D., 1999. Mesozoic Lithostratigraphy. Lithostratigraphic Lexicon of Svalbard. Upper Paleozoic to Quaternary Bedrock. Review and Recommendations for Nomenclature Use, pp. 127–214.

Mulrooney, M.J., Leutscher, J., Braathen, A., 2017. A 3D structural analysis of the Goliat field, Barents Sea, Norway. Mar. Petrol. Geol. 86, 192–212. https://doi.org/10.1016/j.marpetgeo.2017.05.038.

Ohm, S.E., Karlsen, D.A., Austin, T., 2008. Geochemically driven exploration models in uplifted areas: examples from the Norwegian Barents Sea. AAPG (Am. Assoc. Pet. Geol.) Bull. 92, 1191–1223. https://doi.org/10.1306/06180808028.

Riis, F., Fjeldskaar, W., 1992. On the magnitude of the late tertiary and quaternary erosion and its significance for the uplift of Scandinavia and the Barents Sea. In: Larsen, R.M., Brekke, H., Larsen, B.T., Telleraas, E. (Eds.), Structural and Tectonic Modelling and its Application to Petroleum Geology, vol. 1. Norwegian Petroleum Society, Special Publication, pp. 163–185. https://doi.org/10.1016/B978-0-444-88607-1.50016-4.

Riis, F., 1996. Quantification of Cenozoic vertical movements of Scandinavia by correlation of morphological surfaces with offshore data. Global Planet. Change 331–357. https://doi.org/10.1016/0921-8181(95)00027-5.

Rojo, L.A., Escalona, A., 2018. Controls on minibasin infill in the Nordkapp Basin: evidence of complex Triassic synsedimentary deposition influenced by salt tectonics. AAPG Bull. 102 (7), 1239–1272. https://doi.org/10.1306/0926171524316523.

Rojo, L.A., Cardozo, N., Escalona, A., Koyi, H., 2019. Structural style and evolution of the Nordkapp Basin, Norwegian Barents Sea. AAPG (Am. Assoc. Pet. Geol.) Bull. 103 (9), 2177–2217. https://doi.org/10.1306/01301918028.

Scheidt, G., Littke, R., 1989. Comparative organic petrology of interlayered sandstones, siltstones, mudstones and coals in the Upper Carboniferous Ruhr basin, Northwest Germany, and their thermal history and methane generation. Geol. Rundsch. 78, 375–390. https://doi.org/10.1007/BF01988371.

Schlanger, S.O., Jenkyns, H.C., 1976. Cretaceous anoxic events: causes and consequences, Geologie. Mijnbouw 55, 179–184.

Sclater, J., Christie, P., 1980. Continental stretching: an explanation of post mid-Cretaceous subsidence of the central North Sea Basin. J. Geophys. Res. 85, 3711–3739. https://doi.org/10.1029/JB085iB07p03711.

Scotese, C.R., 2016. PALEOMAP PaleoAtlas for GPlates and the PaleoData Plotter Program. PALEOMAP Project. http://www.earthbyte.org/paleomap-paleoatlas-for-gplates/.

Serck, C.S., Faleide, J.I., Braathen, A., Kjølhamar, B., Escalona, A., 2017. Jurassic to early cretaceous basin configuration(s) in the Fingerdjupet Subbasin, SW Barents Sea. Mar. Petrol. Geol. 86, 874–891. https://doi.org/10.1016/j.marpetgeo.2017.06.044.

Smelror, M., Below, R., 1993. Dinoflagellate biostratigraphy of the toarcian to lower Oxfordian (Jurassic) of the Barents Sea region. In: Vorren, T.O. (Ed.), Arctic Geology and Petroleum Potential, vol. 2. NPF special publication, pp. 495–513. https://doi.org/10.1016/B978-0-444-88943-0.50035-6.

Smelror, M., Mørk, A., Mørk, M.B.E., Weiss, H.M., Løseth, H., 2001. Middle Jurassic-Lower Cretaceous transgressive-regressive sequences and facies distribution off northern Nordland and Troms, Norway, 10. Norwegian Petroleum Society Special Publications, pp. 211–232. https://doi.org/10.1016/S0928-8937(01)80015-1.

Sund, T., Skarpnes, O., Jensen, L.N., Larsen, R.M., 1986. Tectonic development and hydrocarbon potential offshore Troms, northern Norway. In: Halbouty, T.H. (Ed.), Future Petroleum Provinces of the World, vol. 40. AAPG Memoir. https://doi.org/10.1306/M40454C29.

Sweeney, R.E., Kaplan, I.R., 1980. Diagenetic sulphate reduction in marine sediments. Mar. Chem. 9, 165–174. https://doi.org/10.1016/0304-4203(80)90035-3.

Tsikalas, F., Gudlaugsson, S.T., Faleide, J.I., Eldholm, O., 1999. Mjolnir Structure, Barents Sea: a Marine Impact Crater Laboratory. Special Papers-Geological Society of America, pp. 193–204. https://doi.org/10.1130/0-8137-2339-6.193.

Tsikalas, F., Blaich, O.A., Faleide, J.I., Olaussen, S., 2021. Stappen High-Bjørnøya Tectono-Sedimentary Element, Barents Sea, vol. 57. Geological Society, London, Memoirs. https://doi.org/10.1144/M57-2016-24.

Weissert, H., McKenzie, J.A., Hochuli, P., 1979. Cyclic anoxic events in the early cretaceous tethys ocean. Geology 7, 147–151. https://doi.org/10.1130/0091-7613(1979)7<147:CAEITE>2.0.CO;2.

Weissert, H., Mohr, H., 1996. Late Jurassic climate and its impact on carbon cycling. Palaeogeogr. Palaeoclimatol. Palaeoecol. 122, 27–43. https://doi.org/10.1016/0031-0182(95)00088-7.

Wierzbowski, A., Smelror, M., 2020. The Bajocian to Kimmeridgian (middle to upper Jurassic) ammonite succession at Sentralbanken high (core 7533/3-U-1), Barents Sea, and its stratigraphical and palaeobiogeographical significance. Volumina Jurassica 18, 1–22. https://doi.org/10.7306/vj.18.1.

Worsley, D., 2008. The post-Caledonian development of Svalbard and the western Barents Sea. Polar Res. 27, 298–317. https://doi.org/10.3402/polar.v27i3.6197.

Zumberge, J., Harold, I., Lowell, W., 2016. Petroleum geochemistry of the cenomanian–turonian eagle Ford oils of south Texas. In: Breyer, J.A. (Ed.), The Eagle Ford Shale: A Renaissance in U.S. Oil Production, vol. 110. AAPG Memoir, pp. 135–165. https://doi.org/10.1306/13541960M110449.